POLITECNICO DI TORINO

Master Thesis in Electrical Engineering

A.Y. 2023/2024

Modeling and Control of Variable Flux PMSM under Asymmetrical Magnetization

Author:

Raffaele Garino

Supervisors:

Paolo Pescetto

Gianmario Pellegrino

Abstract

The rapid advancements in electric mobility and the increasing demand for high-efficiency, high-performance traction systems are driving car manufacturers to explore innovative motor technologies. In this context, Variable Flux Permanent Magnet Synchronous Machines have emerged as a promising alternative to conventional PMSMs, offering improved efficiency and an extended speed range by dynamically adjusting their magnetic flux. This thesis explores the characteristics, modeling, and control of VF-PMSMs, aiming to provide a comprehensive framework for VF-PMSM analysis, contributing to the development of more efficient and adaptable electric drive systems.

The study, conducted as a part of a collaborative research project with Volvo Cars, begins with an overview of VF-PMSMs, detailing their classification and working principles. A case study motor is introduced, followed by the development of its dynamic model. Next, different Simulink-based modeling approaches are presented, with a strong emphasis on magnetization state modeling, which plays a crucial role in capturing the dynamic behavior of the machine and particular effort is devoted to the modeling of the machine under asymmetrical demagnetization, with the fundamental PM flux component deviated with respect to the d-axis.

To validate the developed models, a comparison is conducted between Simulink and JMAG finite element simulations, analyzing key performance metrics such as open-circuit characteristics, demagnetization and remagnetization behavior. Finally, control strategies for VF-PMSMs are investigated, including a modified Field Oriented Control scheme that leverages Magnetization State estimation and consequently adapts the current vector control strategy for improved control performance.

Acknowledgments

First and foremost, I would like to express my deepest gratitude to my supervisors, Paolo Pescetto and Gianmario Pellegrino, for their invaluable guidance, support, and encouragement throughout this journey. Their expertise and insightful advice have been fundamental in shaping this work. I also wish to extend my sincere thanks to all the professors who, throughout these years of study, have contributed to ignite my interest and passion for these subjects.

I would like to express my heartfelt gratitude to all my family, whose unwavering support and belief in me have been a constant source of strength. Especially, I want to thank my parents, without whom this entire journey would not have been possible. Their sacrifices, encouragement, and endless support have been the foundation upon which I have built my academic and personal growth. I am also deeply grateful to my siblings, who have always allowed me to have incredible experiences without ever expecting anything in return. Their generosity and companionship have enriched my life in countless ways.

I am profoundly grateful to my fiancée, Giulia, for her constant presence, understanding, and encouragement. Over these past eight years, she has shared with me not only the big milestones but also the simplest moments, making each one special. I look forward to many more years together, filled with the adventures we have always embraced side by side.

I also extend my sincere appreciation to all my friends and colleagues, valiant companions in this academic odyssey. Together, we have braved countless lectures, study marathons, and the trials of exams, facing them as battles to be fought side by side. The moments of triumph and well-deserved celebrations have made this journey even more memorable.

A special thank you goes to all my lifelong friends, who have been a constant presence throughout the years. In particular, I am profoundly grateful to Mattia and Emanuele, whose friendship and laughter have been invaluable.

This thesis is the result of the collective support and encouragement of all these incredible people, to whom I will always be profoundly thankful.

Index

List of Figures

List of Tables

List of Acronyms

PMSM = Permanent Magnet Synchronous Machine

VF-PMSM = Variable Flux Permanent Magnet Synchronous Machine

PM = Permanent Magnet

SPM = Surface-mounted Permanent Magnet

IPM = Internal Permanent Magnet

SyR = Synchronous Reluctance Motor

PM-SyR = Permanent Magnet assisted Synchronous Reluctance Motor

LCF = Low Coercive Force

HCF = High Coercive Force

FOC = Field Oriented Control

LUT = Look-up Tables

b-EMF = Back electromotive force

MTPA = Maximum Torque Per Ampere

Introduction and Motivation

The global push for decarbonization and the transition to fully electric mobility are driving rapid advancements in electric motor technology. As industries strive to reduce carbon emissions and move away from fossil fuels, high-performance electric machines are gaining attention for their superior efficiency, controllability, and adaptability. These innovations are essential for enabling cleaner transportation and accelerating the shift toward sustainable energy solutions. One such emerging category is the Variable Flux Permanent Magnet Synchronous Motor. Unlike conventional Permanent Magnet Synchronous Motors, VF-PMSMs allowing for magnet flux variation, enabling greater flexibility in performance optimization across different operating conditions. This characteristic makes them particularly suitable for applications that require a wide speed range, improved efficiency, and enhanced controllability.

This thesis, conducted as a part of a collaborative research project with Volvo Cars, aim to develop an accurate yet efficient model for VF-PMSMs to streamline control strategy development, it seeks to balance precision and speed, bridging the gap between detailed but slow finite element models and simplified analytical approaches.

Building on this foundation, the second part focuses on developing an estimator for the new quantities introduced by the model: the Magnetization State and it's phase, enabling better real-time monitoring and control of VF-PMSMs. To fully leverage these new variables, the Field Oriented Control is modified

1 Variable Flux PMSM

Permanent Magnet Synchronous Machines have gained widespread popularity in electric drive applications due to their high efficiency, power density, and robust performance. However, conventional PMSMs face challenges in achieving a wide speed range efficiently, as they rely on flux weakening strategies that require additional current to counteract the permanent magnet flux, leading to increased losses and reduced efficiency at high speeds. To overcome these limitations, Variable Flux Permanent Magnet Synchronous Machines have been introduced. This chapter explores the different types of VF-PMSMs, followed by the structural characteristics of the case study motor, and finally presents the dynamic model used in the subsequent chapters.

1.1 Type of VF-PMSM and generalities

VF-PMSMs are a relatively new class of electrical machines, first proposed in 2001[6], characterized by the ability to dynamically adjust their flux without resorting to normal flux weakening strategies. The idea behind this type of machine is that traditional PMSMs with strong Permanent Magnets, meaning high magnetic flux, offer high torque in compact size machines, but this means that for flux weakening, it is necessary to use significant current to counteract the magnet flux, increasing the losses and resulting in a low flux weakening range with reduced efficiencies. Although machines with a weaker magnet flux have a minor torque density but an increased flux weakening capability.VF-PMSMs aim to integrate these characteristics by introducing an additional degree of freedom, represented by the magnetization state, utilizing a high magnetic flux at low speeds to achieve high torque and reducing flux at high speeds. This flux adjustment eliminates the need to actively counteract the magnet flux, improving efficiency.

VF-PMSMs can be divided into three categories[2]: Low Coercive Force permanent magnets only, Hybrid-excitation and Mechanically adjusting rotor's structure.

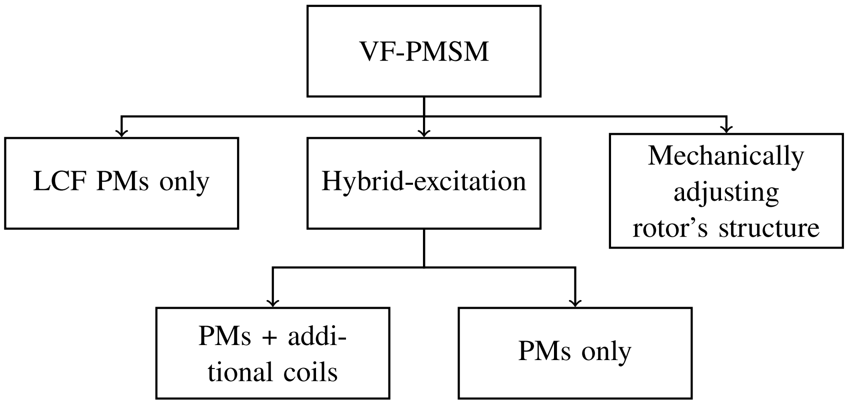

Figure 1.1: Categorization of VF-PMSMs

1.1.1 LCF PMs only

These types of VF-PMSMs, generally speaking, are constructively the simplest one, because they feature the same stator and rotor structure as a normal PMSM and differ only for the type of magnet used, which are Low Coercive Force Permanent Magnet.

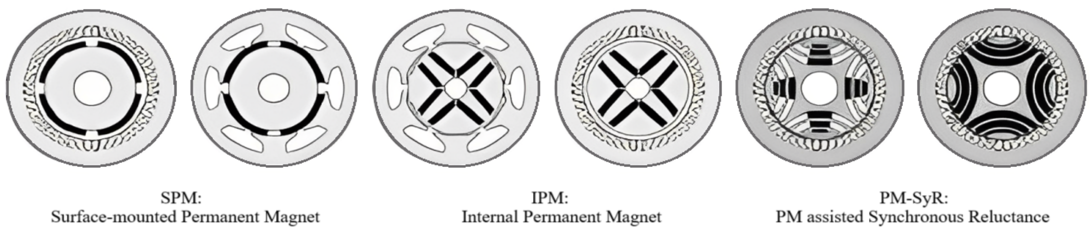

Figure 1.2: Types of PMSMs

LCF PMs are a class of magnets also referred as soft magnets, that can lose or gain magnetization easily, because is sufficient a small external magnetic field to change their magnetization state, being the coercive force the measure of the ability of a ferromagnetic material to withstand an external magnetic field without becoming demagnetized. The most commonly used are [4] AlNiCo, SmCo and ferrite, with the first generally featuring the lowest coercivity between the three.

These magnetic features are used to achieve this class of VF-PMSMs varying the magnetization state through current pulses, increasing the operative area of the motor maintaining a higher efficiency.The possible downside of this kind of VF-PMSMs is the risk of on-load unintentional demagnetization due to armature reaction fields.

To mitigate the risk of on-load unintentional demagnetization while relying solely on LCF PMs, alternative motor structures have been explored. One such approach is inverted saliency

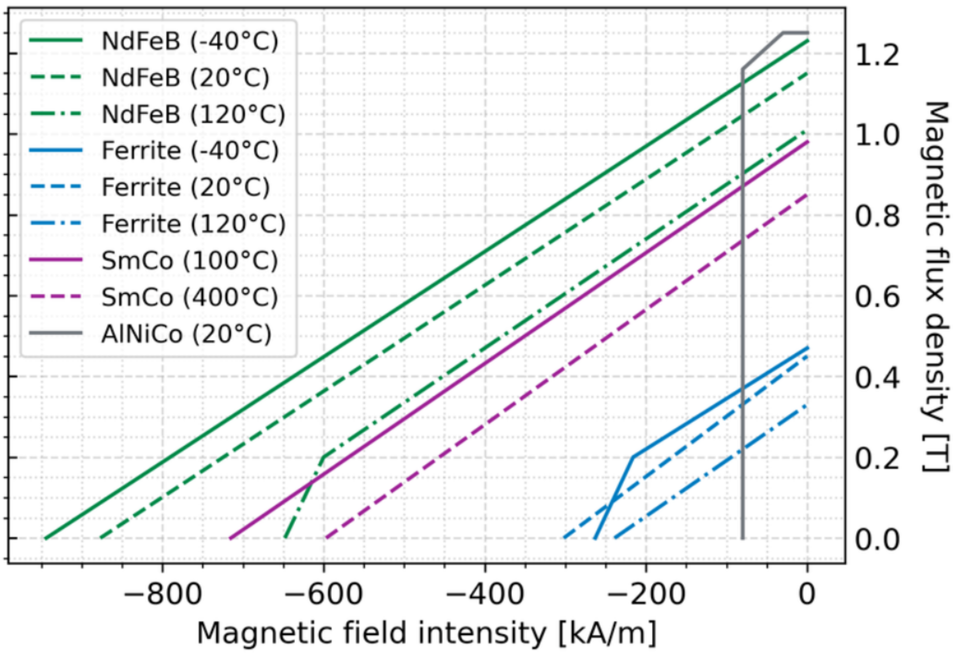

Figure 1.3: Magnet demagnetization curves

designs[3], characterized by $L_d > L_q$, which help enhance stability and reduce undesired demagnetization effects.

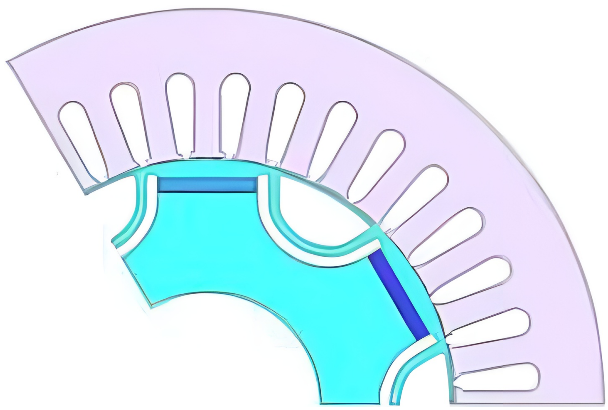

Figure 1.4: Inverted saliency VF-PMSMs [3]

1.1.2 Hybrid-excitation

This type of VF-PMSM is divided in two subcategories, one that combines HCF and LCF magnets and the other that uses HCF magnets and additional field coils. For both the basic idea is the same, meaning using HCF magnets, such as NdFeB, to have a base magnetic field and than have another source of magnetic field that is controllable, the first solution through magnetization and demagnetization of the LCF PMs, while the second through additional coils.

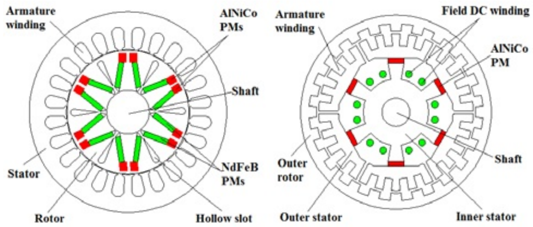

Figure 1.5: Example of hybrid-excitations VF-PMSMs [2]

These types of VF-PMSM are less sensitive to involuntary demagnetization, decreasing the degree of freedom to manage the magnetization state.

1.1.3 Mechanically adjusting rotor's structure

These last class of VF-PMSMs uses centrifugal force, or other strategies, to change the rotor structure while spinning, inducing a reduction of the flux through the air gap. Although it is a VF-PMSM, the magnetic flux control is strictly related to the speed and acceleration of the motor, significantly reducing the degree of freedom of control.

1.2 Structure of the motor under test

The VF-PMSM considered for this work features a three-pole pairs SPM rotor structure with AlNiCo 5 magnets, featuring a slightly anisotropy. A prototype of this machine is currently under manufacturing, targeting an experimental validation of the developed modeling and control techniques. The SPM structure was chosen attempting to reduce the remagnetization current, and for manufacturing simplicity.

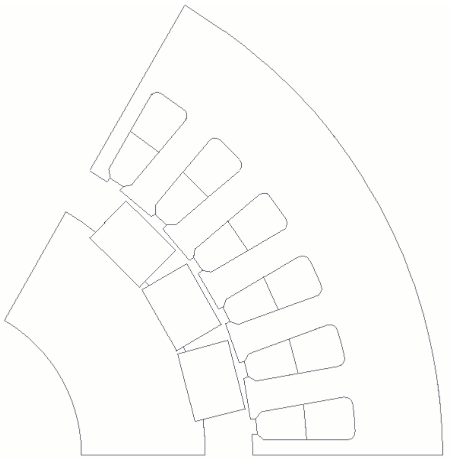

Figure 1.6: Motor geometry

Specification	Value
Topology	SPM
Pole pairs	3
Magnet	AlNiCo 5 magnets
I_n	19 A
$T_n(MS = 80\%)$	35 Nm
$\omega_n(MS = 80\%)$	2700 rpm
$T_n(MS = 40\%)$	18 Nm
$\omega_n(MS = 40\%)$	3850 rpm
DC-link V_n	565 V
ω_{MAX}	10000 rpm

Table 1.1: Motor specifications

The motor, enabling the variation of the magnetization state, allows for achieving both high torque at high MS and high speeds at low MS values.

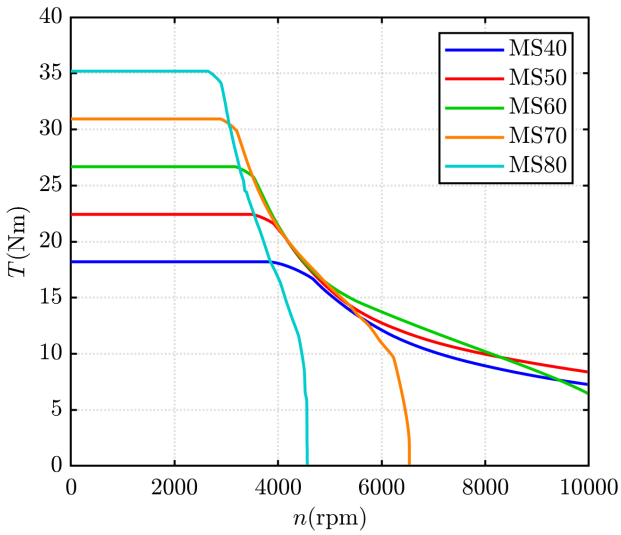

Figure 1.7: Motor under test Torque-Speed characteristic

1.3 Dynamic model for VF-PMSM

VF-PMSMs can all be modeled in the *abc* phase coordinates, by an electrical equation:

$$\boldsymbol{v}_{abc} = R_s \cdot \mathbf{i}_{abc} + \frac{d\boldsymbol{\lambda}_{abc}}{dt} \tag{1}$$

Where $\mathbf{v}_{abc}$ is the voltage vector, $\mathbf{i}_{abc}$ the current vector, and R_s is the stator winding resistance and λ_{abc} the flux linkage vector, defined by the magnetic equation:

$$\boldsymbol{\lambda}_{abc} = \mathbf{L}_{abc}(\theta_r) \cdot \mathbf{i}_{abc} + \boldsymbol{\lambda}_{m,abc}(\theta_r) \tag{2}$$

Where $\boldsymbol{L}_{abc}(\theta_r)$ is the self and mutual inductance matrix, and $\boldsymbol{\lambda}_{m,abc}(\theta_r)$ is the permanent magnet flux linkage. The torque equation results:

$$T_e = \frac{p}{2}\left(\mathbf{i}_{abc}^T \cdot \frac{\partial \mathbf{L}_{abc}(\theta_r)}{\partial \theta_r} \cdot \mathbf{i}_{abc} + \mathbf{i}_{abc}^T \cdot \boldsymbol{\lambda}_{m,abc}(\theta_r)\right) \tag{3}$$

In the *abc* reference system voltages, fluxes and currents are sinusoidal and time-varying quantities, making them complex for analysis and control purposes, so instead the rotating *dq* reference frame is used, transforming the sinusoidal quantities in to steady-state variables. The conversion is done by using the Clarke transform *abc* $\rightarrow \alpha\beta$:

$$[T] = \frac{2}{3}\begin{bmatrix} 1 & -\frac{1}{2} & -\frac{1}{2} \\ 0 & \frac{\sqrt{3}}{2} & -\frac{\sqrt{3}}{2} \end{bmatrix} \tag{4}$$

For machine modeling a crucial role is played by the voltage equations in the $\alpha\beta$ reference system, because, when inverted, they are used to compute the flux components in the motor model.

$$\boldsymbol{v}_{\alpha\beta} = R_s \cdot \mathbf{i}_{\alpha\beta} + \frac{d\boldsymbol{\lambda}_{\alpha\beta}}{dt} \tag{5}$$

once inverted became:

$$\frac{d\boldsymbol{\lambda}_{\alpha\beta}}{dt} = \boldsymbol{v}_{\alpha\beta} - R_s \cdot \mathbf{i}_{\alpha\beta} \tag{6}$$

allowing to calculate the flux as:

$$\boldsymbol{\lambda}_{\alpha\beta} = \int \boldsymbol{v}_{\alpha\beta} - R_s \cdot \mathbf{i}_{\alpha\beta}\, dt \tag{7}$$

Then the rotation transform $\alpha\beta \rightarrow$ dq:

$$[A(\theta_e)] = \begin{bmatrix} \cos(p\cdot\theta_r) & \sin(p\cdot\theta_r) \\ -\sin(p\cdot\theta_r) & \cos(p\cdot\theta_r) \end{bmatrix} \tag{8}$$

The definition of the rotating dq reference frame may vary depending on the type of PMSM, aligning the d axis to the direction of the magnets, PM-style used for SPM and IPM, or aligning it to the direction of maximum inductance, SyR-style used for SyR and PM-SyR. The dq dynamic

Figure 1.8: dq reference frame style

model results to be:

$$\boldsymbol{v}_{dq} = R_s \cdot \mathbf{i}_{dq} + \frac{d\boldsymbol{\lambda}_{dq}}{dt} + [\boldsymbol{J}] \cdot \omega \cdot \lambda_{dq} \tag{9}$$

where $J = \begin{bmatrix} 1 & 0 \\ 0 & 1 \end{bmatrix}$ and ω the electrical frequency.

$$\boldsymbol{\lambda}_{dq} = [\mathbf{L}_{dq}] \cdot \mathbf{i}_{dq} + \boldsymbol{\lambda}_{m,dq} \tag{10}$$

In reality, however, due to the effects of magnetic saturation and cross-coupling, the flux linkage is a non-linear function of the currents, as for other normal PMSMs, but also of the state of magnetization, constituting the peculiarity of the Variable Flux machines[5].

$$\begin{cases} \lambda_d = \lambda_d(i_d, i_q, MS) \\ \lambda_q = \lambda_q(i_d, i_q, MS) \end{cases} \tag{11}$$

$$\begin{cases} \lambda_m = \lambda_d(i_d = 0, i_q = 0, MS) \\ MS = \dfrac{\lambda_m}{\lambda_{m,MAX}} \end{cases} \tag{12}$$

The torque equations results:

$$T_{em} = \frac{3}{2} \cdot P \cdot (\lambda_d(i_d, i_q, MS) \cdot i_q - \lambda_q(i_d, i_q, MS) \cdot i_d) \tag{13}$$

The motor under test exhibits minimal saturation and has an almost constant inductance. Therefore, this will be the initial approach in the modeling process, using linearized equations to describe the dynamic behavior. Subsequently, the model will be refined by incorporating saturation and cross-saturation effects, using a maps based model. The mathematical framework used for modeling the M.U.T. will be explored in greater detail in the dedicated chapter.

2 Simulink model of the VF-PMSM

Accurate modeling of VF-PMSMs is essential for analyzing their dynamic performance and developing effective control strategies. Given the magnetization state variation capability of these machines, conventional PMSM models are insufficient, requiring more advanced modeling to represent the effect of variable magnetization on machine behavior. This chapter presents the development of a Simulink-based VF-PMSM model, beginning with the introduction of the simulation environment, continuing with the presentation of the baseline model on which the successive refining are built, to account for uneven demagnetization and remagnetization.

2.1 Simulation environment

Before the analysis of the actual motor model and its evolution it is necessary to introduce the syreDrive environment, that is part of the SyR-e[8], that stand for Synchronous Reluctance - evolution, an open source Matlab/Octave package, released in 2014 by a collaboration project between the Politecnico di Torino and the Politecnico di Bari.

Created and continuously updated as a motor design tool based on FEA and multi-objective optimization algorithms for Synchronous Reluctance machines, over time it has evolved to be able to manage any type of electric motor, and furthermore allowing magnetic model manipulation, like computing inverse flux maps or inductance maps starting from the direct flux maps, and more, a fundamental feature for both modeling and control of the machines.

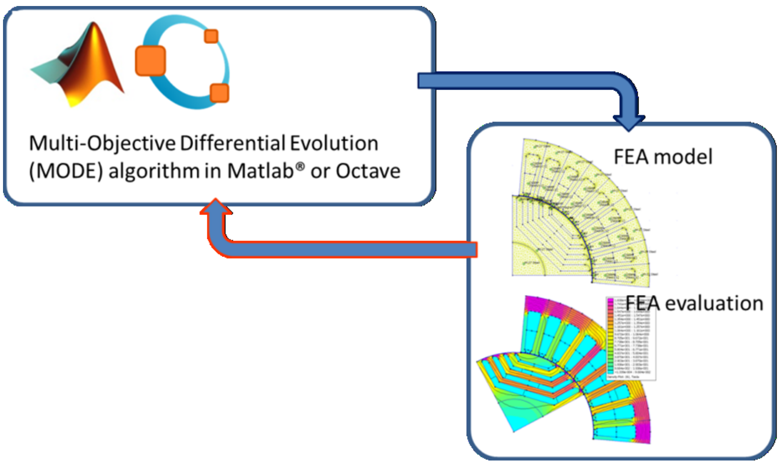

Figure 2.1: SyR-e data flow

Starting from 2021 [9] it also integrate the syreDrive a tools that automatically generate a control simulation environment in Simulink or Plecs, through a simple interface that allow to chose the motor and model type, the type of control, the converter model characteristics and even the specification of an automatically generated control code.

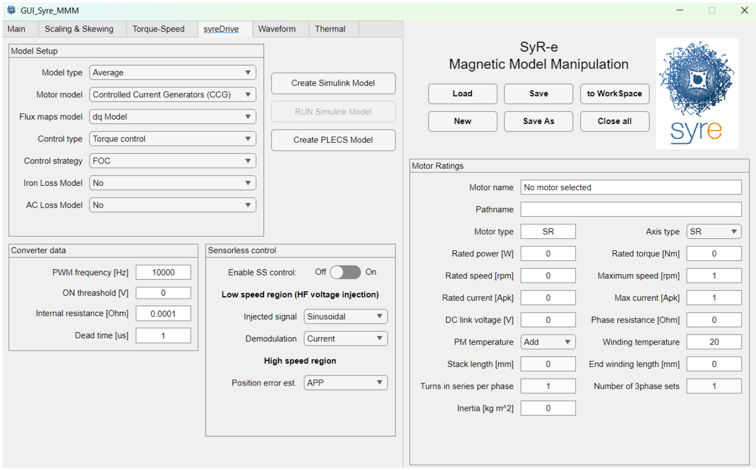

Figure 2.2: syreDrive interface

In this work, the SyR-e Simulink environment has been used as the framework for both machine modeling and control.

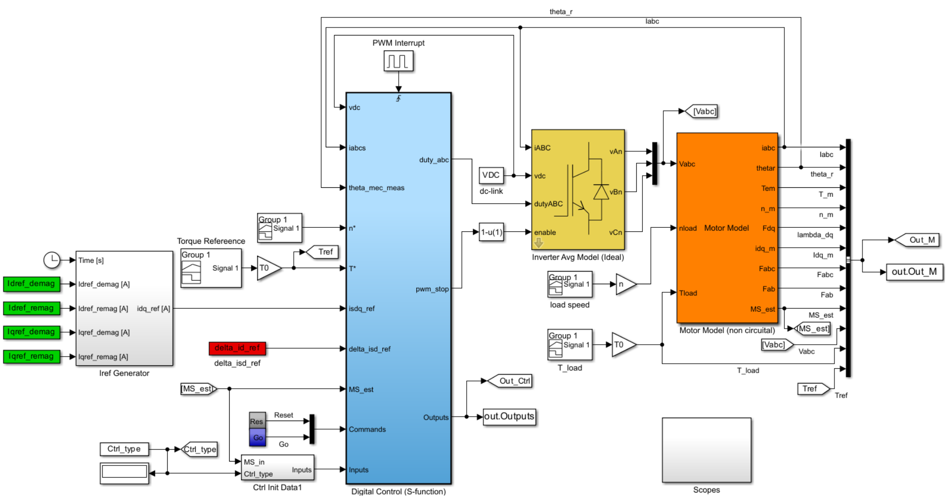

Figure 2.3: Simulink syreDrive environment

It is divided in three main blocks: the first is the digital control block, the blue one, it represents a microcontroller, where the control code is loaded. This block manages inputs and outputs as if it were a physical microcontroller, utilizing a PWM interrupt block to generate interrupt service routine signals, thereby enabling real-time operation simulation.

Following the microcontroller block, there is the inverter block, the yellow one, that receives the duty cycle signals from the microcontroller. This block processes the signals and generates the corresponding output voltage, effectively simulating the behavior of a real inverter.

The last block in the, the orange one, represents the actual motor. It receives the output voltage from the inverter block and simulates the electromechanical behavior of the machine, providing feedback such as current, speed, and position, which can be used for control and analysis.

The following section will focus on the motor model within the Simulink environment.

2.2 Initial motor model

The baseline model used as starting point, presented in 2024[5], is an already high-fidelity model for control simulation, that represent a great evolution respect to time-consuming co-simulation coupled with FE analysis.The model is based on Look-up Tables pre-calculated in FEA, like most of the normal PMSMs, but beside the inverse flux LUTs, that are calculated for different MS, it features two additional LUT that account for De-magnetization and Re-magnetization behavior.

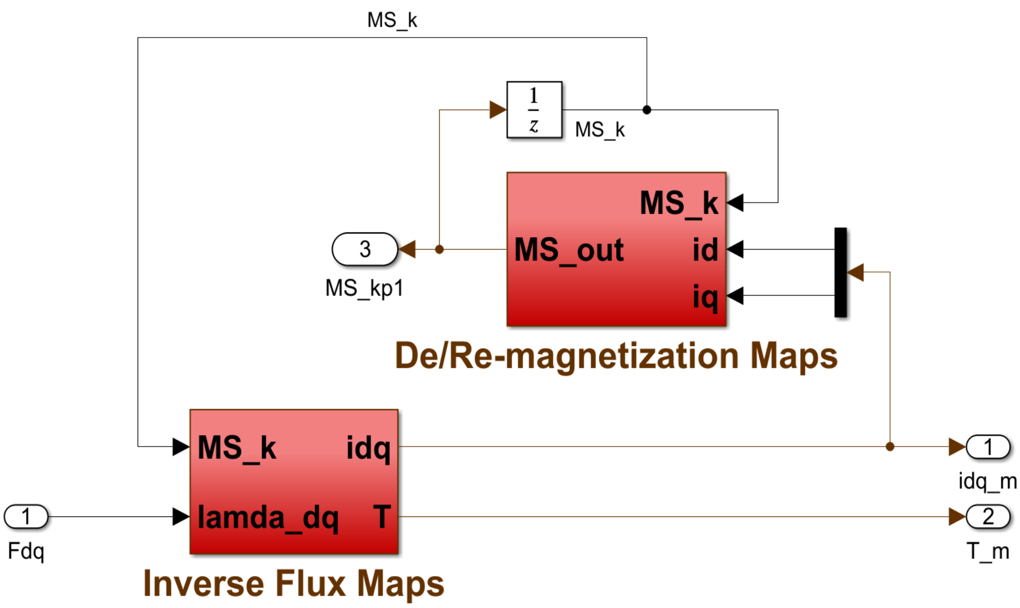

Figure 2.4: VF-PMSM initial High-level electromagnetic model

At each simulation step, the flux components in the $\alpha\beta$ reference frame $\lambda_{\alpha\beta}$ are computed using (7). These flux components are then transformed into dq reference frame, λ_{dq}, using the rotational transform n(8). Once in the dq domain, the fluxes, are used in the inverse flux maps to determine the corresponding current components i_{dq}, the inverse flux maps are computed at different levels of MS, to account fot PM demagnetization. These current values are then passed through the De/Re-magnetization maps, where the MS is retrieved. The MS value is stored using a delay block, ensuring that it is available for the next simulation step, where it is used again in the inverse flux maps.

2.2.1 De/Re-magnetization MAPS

The demagnetization and remagnetization maps are the core blocks of this innovative model. The idea behind is that a large current in the negative d-axis can demagnetize the PMs and at the opposite in the positive direction can remagnetize them. To take this phenomenon into account, two maps in the dq current domain have been created, through FE analysis, following the relations expressed in (12).

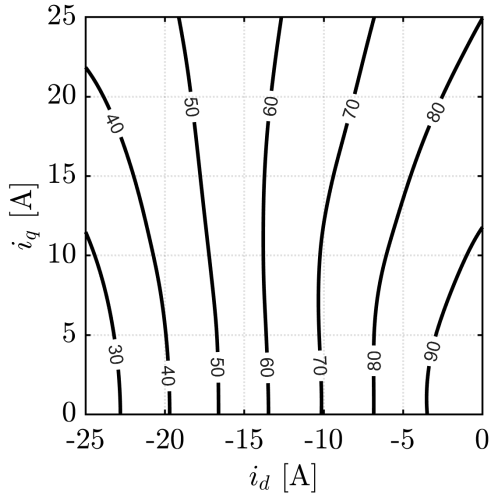

Figure 2.5: De-magnetization map

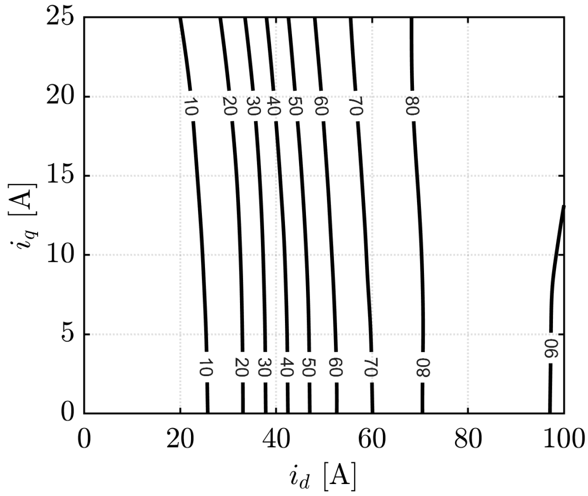

Figure 2.6: Re-magnetization map

The De-magnetization map, represented in Figure$\sim$ 2.5, begins at $i_{dq} = 0$ with an initial magnetization state of 100%. As the current moves into the second quadrant, the MS diminishes, indicating that the VF-PMSM is undergoing demagnetization. Consequently, the demagnetization map indicates, per each point of the second quadrant, the corresponding MS reached by the machine when starting from full magnetization. Conversely, the Re-magnetization map, showed in Figure~ 2.6, start with fully demagnetized PMs, meaning MS=0%. As the current i_d increases in the first quadrant, the map determines the extent to which the VF-PMSM is remagnetized.

In the model, at each simulation step, the current components (i_d,i_q) are input to both maps, as showed in Figure~2.7, An algorithm then evaluates the operating conditions and determines which map is appropriate to use. If the motor is in a demagnetization state, the De-mag. map is applied, reducing the MS. On the other hand, if the conditions indicate remagnetization, the Re-mag. map is selected, increasing the MS accordingly.

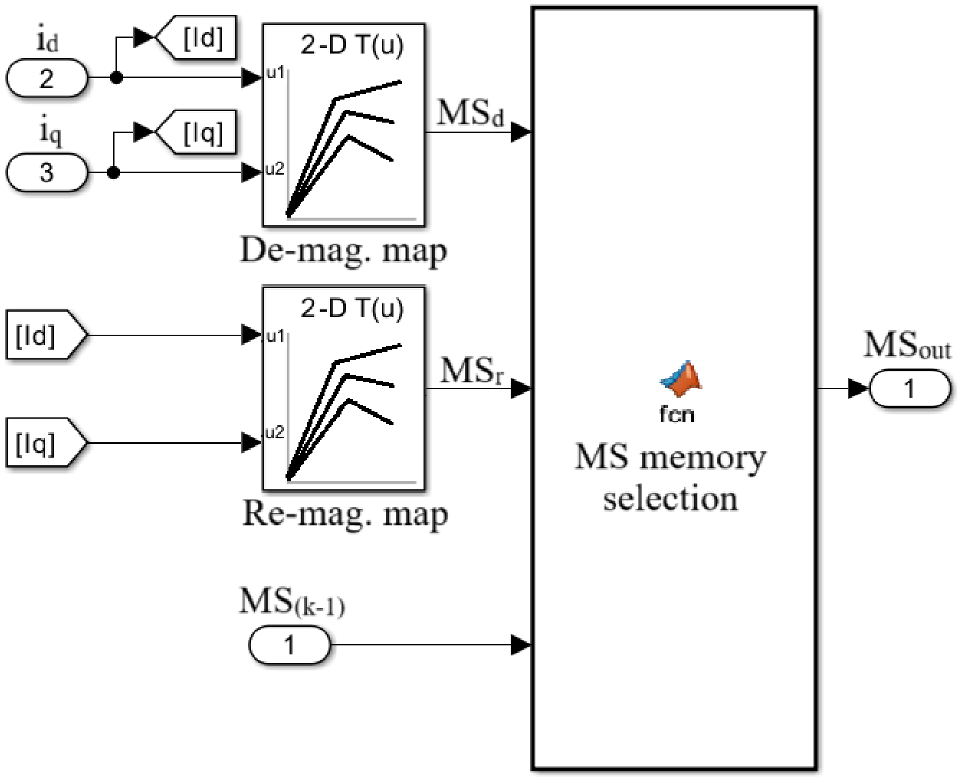

Figure 2.7: De/Re-mag maps model

The MS value decision-making algorithm, which determines the correct value from the output of the De-mag. and Re-mag. maps, is represented in the flow chart 2.8. Furthermore, this also explains the necessity of the delay block shown in Figure2.4. Since the decision depends on previous values of MS, a delay block is required to store and reference past data, ensuring the correct selection at each step.

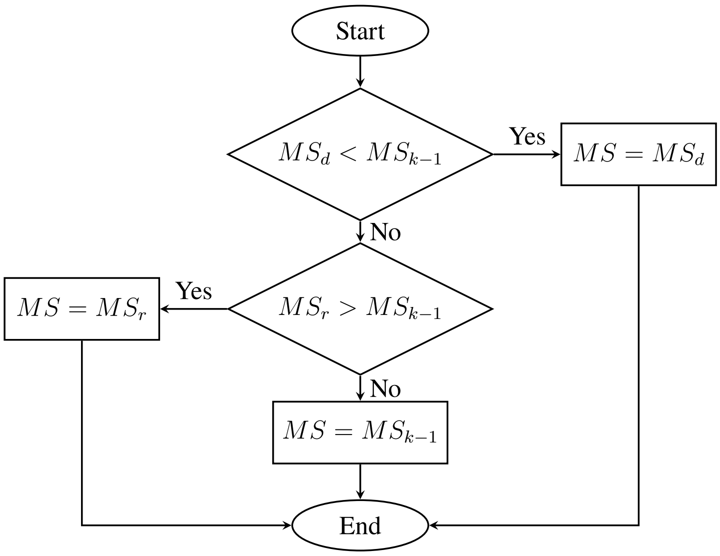

Figure 2.8: MS selection algorithm flow chart

Where MS_d and MS_r are respectively the output of the demagnetization and remagnetization map.

2.2.2 Magnetic model

As discussed in the previous chapter, this type of machine is described by a nonlinear magnetic relationship due to magnetic saturation and cross-coupling. Consequently, the magnetic model must be represented using LUTs. Introducing the MS as an additional degree of freedom requires multiple map, ideally one for each MS value, however, this approach would be computationally impractical, as the advantages gained would not justify the increased computational burden.Instead, the maps are computed for a selected set of discrete MS values, and linear interpolation is used to estimate the values for intermediate cases, as showed in Figure$\sim$2.9 ,where the flux maps where obtained for two MS values (40%, 80%).

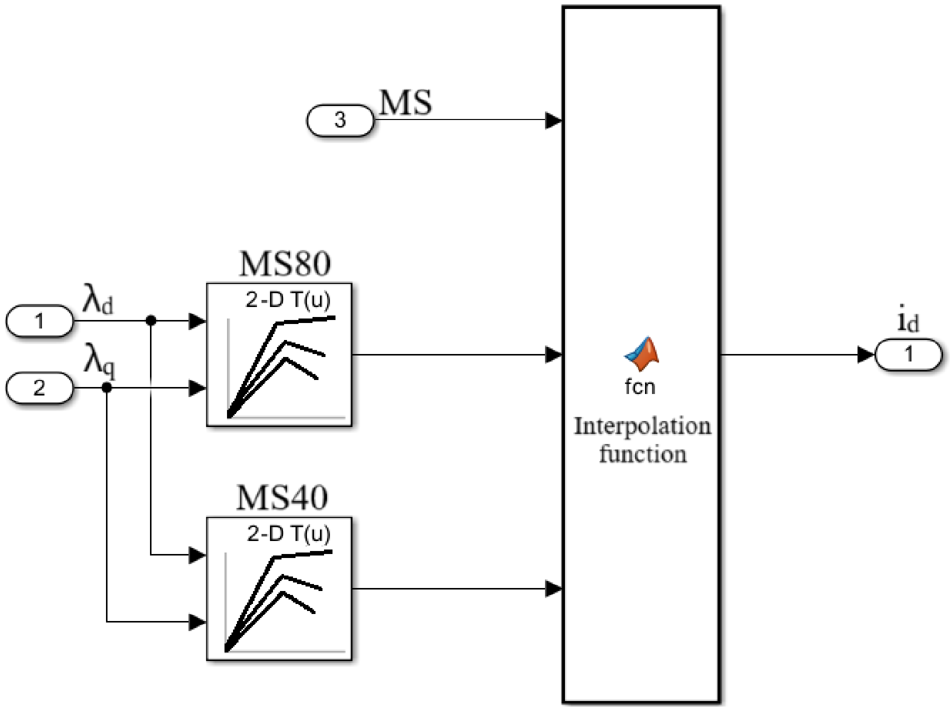

Figure 2.9: d-axis magnetic model

In general, 3D LUTs can be adopted, with the current determined as a function of $\lambda_{\mathbf{dq}}$ and MS.

2.3 Unevenly De/Re-magnetization motor model

As previously mentioned, the baseline model described is an already high-fidelity model for the representation of a VF-PMSM. However, it has a key limitation: it assumes that the PMs are always evenly magnetized, in contrast, FE analysis has shown that magnetization can vary depending on the current pulse, particularly when there is a significant current component along the q-axis, some of the magnetic domains experience greater demagnetization than others, leading to uneven magnetization of the PMs, as shown in Figure~2.10.

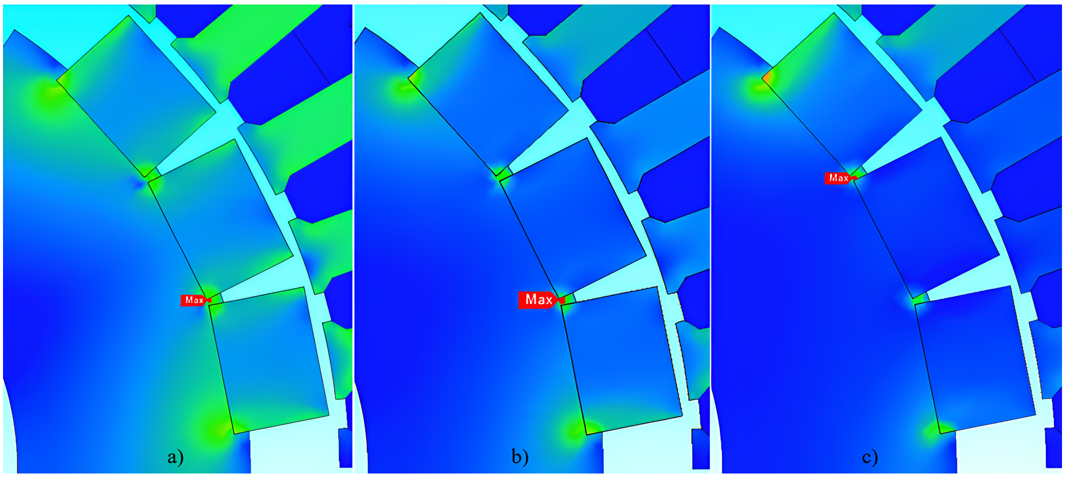

Figure 2.10: Demagnetization comparison: a) PMs at MS=100%, b) PMs at MS=55% evenly magnetized ($i_d = -15A$,$i_q = 0A$), c) PMs at MS=57% unevenly magnetized ($i_d = -15A$,$i_q = 15A$)

This non-uniformity affects the overall flux distribution and can influence machine performance, making it an important factor to consider in modeling. In a first analysis this phenomenon results to be significant for the qd reference frame, as it affects the direction of the magnet flux vector, making it misaligned from the d-axis, creating a q-component of the magnetic flux. In the case of dq reference frame misalignment, several negative effects can occur, significantly impacting the motor performance. These can include the loss of effective torque control due to improper decoupling of the axis, leading to reduced efficiency and dynamic response. Furthermore, it may introduce oscillations and instability, particularly in high-speed applications.

Further analysis has revealed that, additional problem arise due to the method used to model the phenomenon rather than the phenomenon itself. In particular, when evaluating demagnetization using the isoline of magnetization state, the overall magnetization state can appear lower than the one of the isoline. For example if the PMs undergo an initial demagnetization with an high current component in the q-axis, this may results in a magnet that has primarily lost demagnetization in its upper region. If a second current pulse, on the same isoline but with a lower or negligible i_q, further demagnetize the magnet. Despite the system remaining on a specific demagnetization isoline, the cumulative effect of sequential demagnetization events leads to a lower overall magnetization state than what would be expected based solely on the De/Re-magnetization maps.

These phenomena becomes negligible if demagnetization and remagnetization are considered only through the d-axis current component. However, such an assumption contradicts the fundamental principle of VF-PMSMs, which rely on dynamically adjusting the magnetization state during normal operation. Since i_q is actively used to produce torque, variations in magnetization occur under both d- and q-axis current components, making it essential to account for their combined effects.

2.3.1 Unevenly De/Re-magnetization maps

To model the previously described phenomenon, it is necessary to determine the direction of the magnet flux vector. This allows us to identify the new alignment in the presence of uneven magnetization. To achieve this, new de-magnetization and re-magnetization maps have been computed. While maintaining the same MS values, a new quantity—the phase of the back electromotive force at open circuit, has been introduced.Since the b-EMF space vector is in quadrature with the magnet flux vector, it provides a means to determine the actual position of the fundamental component of the PM flux linkage in cases of uneven magnetization of the permanent magnets.

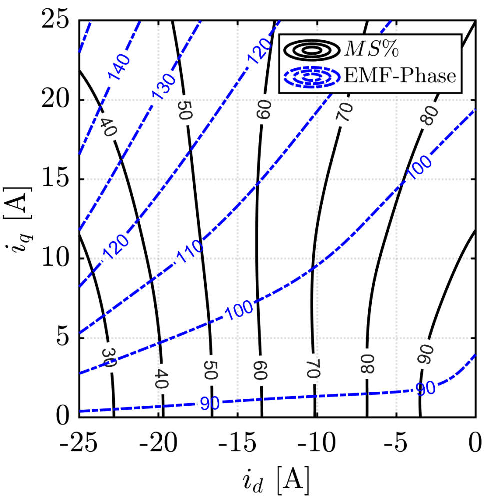

Figure 2.11: De-mag. map with phase

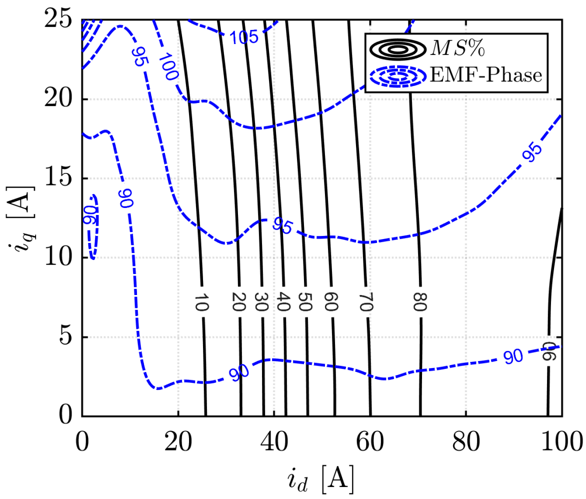

Figure 2.12: Re-mag. map with phase

However, these maps do not account for the cumulative effect of multiple instances of uneven demagnetization or remagnetization. To account for this phenomenon, the magnet was modeled as two equivalent magnets instead of treating it as a single entity, as done in the maps, allowing for a more accurate representation of the cumulative effect of multiple uneven demagnetization or remagnetization.

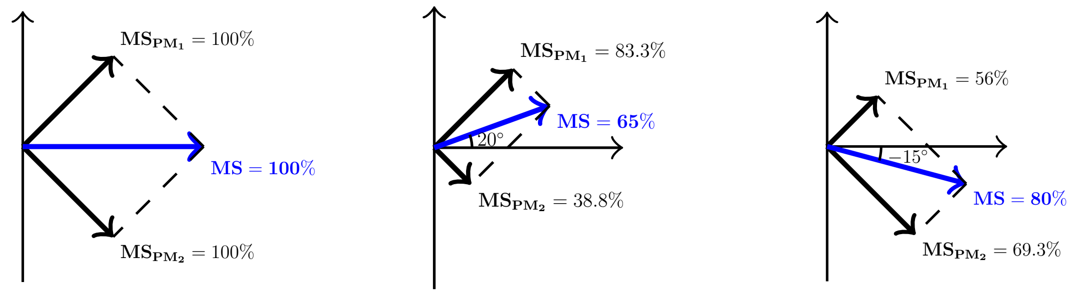

Figure 2.13: Vectorial representation of the equivalent magnets

The basic idea to account for he cumulative effects of multiple uneven demagnetization and remagnetization events, is to represent the magnet as two components in quadrature, at fixed angles respectively +45° and -45°. The ±45° angles have been chosen arbitrarily, since this representation allows to maintain a physical behavior of demagnetization and remagnetization of the equivalent magnets. However, since this is a mathematical model, it can potentially work correctly with any angle as long as the components remain in quadrature, but this topic has not been explored in depth.

The working principle is that Each pulse affects the two components differently based on the magnitude and direction of the unevenness. For example, if an initial pulse demagnetizes the first component by 50% and the second by 80%, a successive pulse, when applied using conventional mapping, might incorrectly suggest partial remagnetization of the first component. However, this contradicts the physical reality that a demagnetization pulse cannot remagnetize a previously weakened region. By modeling the magnet as two independent components, the correct cumulative effect is preserved. Continuing with the example, if the second pulse results in an updated demagnetization of 55% for the first component and 40% for the second, the model correctly maintains the first component at 50% and the second at 40%, ensuring that the system's evolution follow the physical constraints of magnetization processes.

To implement this solution in the motor model, it is necessary to generate Re-magnetization and De-magnetization maps for both equivalent magnets. These maps are derived from the original ones using the following equations:

$$
\begin{cases}
MS_{phase,i,j} = \angle EMF - \dfrac{\pi}{2} \\
MS_{PM1,i,j} = \dfrac{MS_{i,j} \cdot \cos\left(MS_{phase,i,j}\right) + MS_{i,j} \cdot \sin\left(MS_{phase,i,j}\right)}{\sqrt{2}} \\
MS_{PM1,i,j} = \dfrac{MS_{i,j} \cdot \cos\left(MS_{phase,i,j}\right) + MS_{i,j} \cdot \sin\left(MS_{phase,i,j}\right)}{\sqrt{2}}
\end{cases}
\tag{14}
$$

With the re-magnetization and de-magnetization maps successfully generated, the subsequent step involves their integration into the motor model.

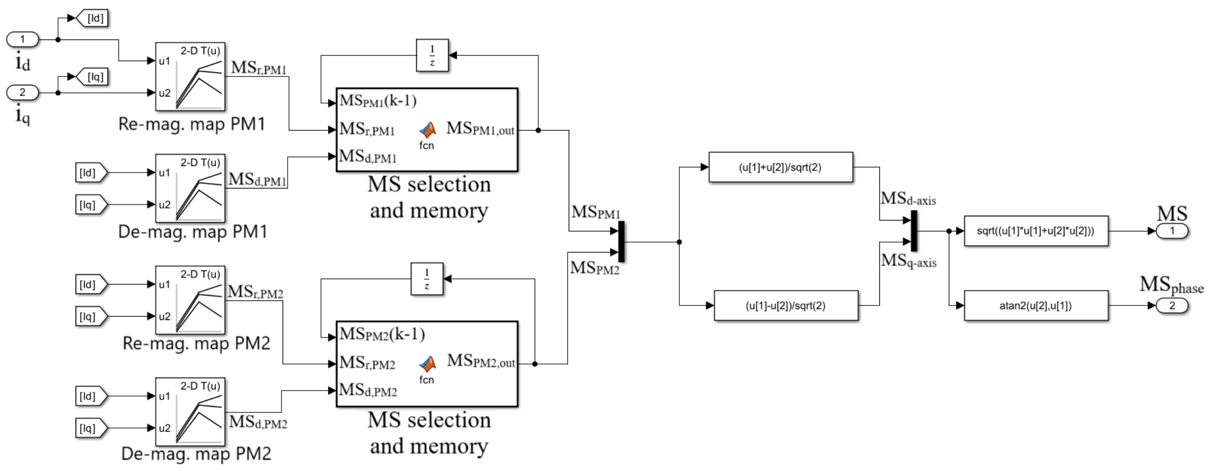

Figure 2.14: Uneven De/Re-magnetization model

The initial structure for each magnet remains the same as shown in Figure~2.7. The algorithm in Figure~ 2.8 is used to select the appropriate MS_{PM} value between demagnetization and remagnetization while storing it in memory. Furthermore, once MS is computed for each equivalent magnet, the overall MS and MS_{phase} are computed.

At a higher level, the system remains equivalent to the initial one, Figure~2.4, supported by the newly introduced quantities represented by the MS_{phase}.

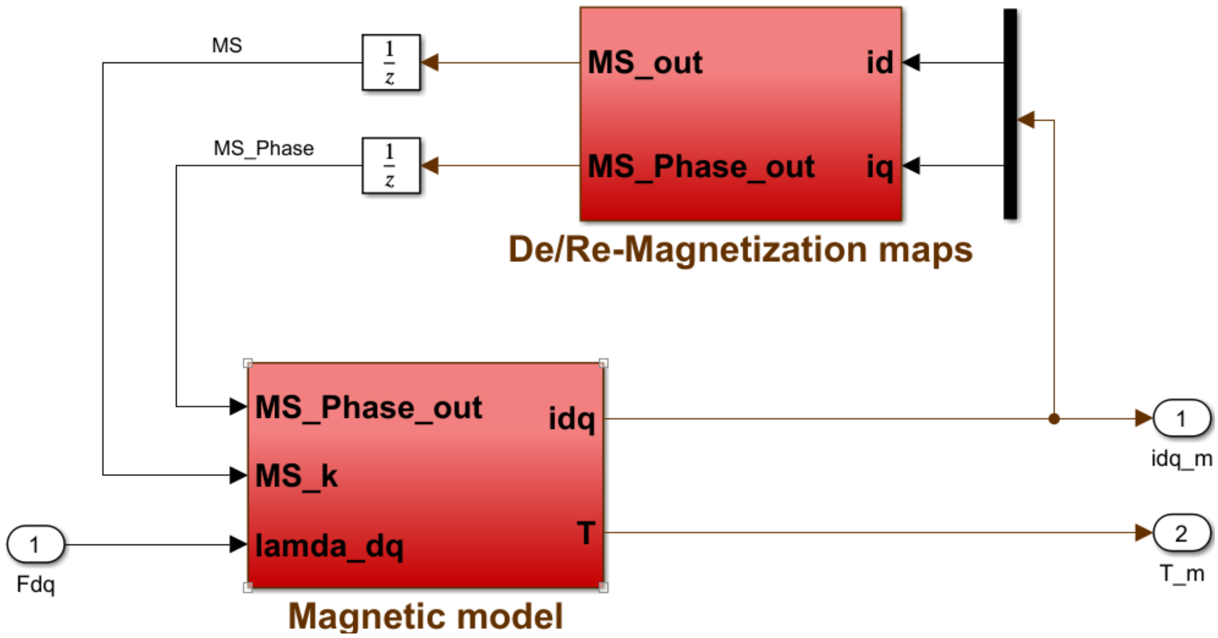

Figure 2.15: VF-PMSM new High-level electromagnetic model

2.3.2 Constant inductance magnetic model

In the initial model, the magnetic relation are represented using inverse flux maps. However, this approach already presented a significant computational burden, as it required generating multiple maps, for different values of MS. In the new model, following the same path results to be impractical, because an excessive number of maps would be needed to account for various demagnetization scenarios, needing to compute maps at different MS values for a sufficient number of MS_{phase} value. For instance, maintaining the same number of magnetization states as in the initial model: 40% and 80% while also accounting for, at least the same values, of MS_{phase} cases would require a total of six maps for each of the dq axes. This makes the direct application of inverse flux maps unfeasible for the new model.

Given the complexity and impracticality of managing such a large number of flux maps, the first adopted solution was to transition to a simplified, linearized magnetic model, with constant inductances. Since the motor geometry is a SPM type, the dynamic model used for the dq-axis representation follows the standard formulation for SPM machines adapted for this specific case of variable flux motor.

The standard formulation of the magnetic model for an SPM motor is:

$$\begin{cases} \lambda_d = L_d \cdot i_d + \lambda_m \\ \lambda_q = L_q \cdot i_q \end{cases} \tag{15}$$

$$\begin{cases} \lambda_{dm} = \lambda_m \\ \lambda_{qm} = 0 \end{cases} \tag{16}$$

To adapt the standard SPM model to the VF-PMSM in study, the equations become:

$$\begin{cases} \lambda_d = L_d \cdot i_d + \lambda_{dm} \\ \lambda_q = L_q \cdot i_q + \lambda_{qm} \end{cases} \tag{17}$$

Adapting the 12 and introducing the MS_{phase} the final magnetic model become:

$$\begin{cases} \lambda_d = L_d \cdot i_d + MS \cdot \lambda_{m,MAX} \cdot \cos\left(MS_{phase}\right) \\ \lambda_q = L_q \cdot i_q + MS \cdot \lambda_{m,MAX} \cdot \sin\left(MS_{phase}\right) \end{cases} \tag{18}$$

Once inverted, it can be used in the actual motor model, retrieving the λ_{dq} values from the same integral relation7.

$$\begin{cases} i_d = \dfrac{\lambda_d - MS \cdot \lambda_{m,MAX} \cdot \cos\left(MS_{phase}\right)}{L_d} \\ i_q = \dfrac{\lambda_q - MS \cdot \lambda_{m,MAX} \cdot \sin\left(MS_{phase}\right)}{L_q} \end{cases} \tag{19}$$

The implemented model results to be:

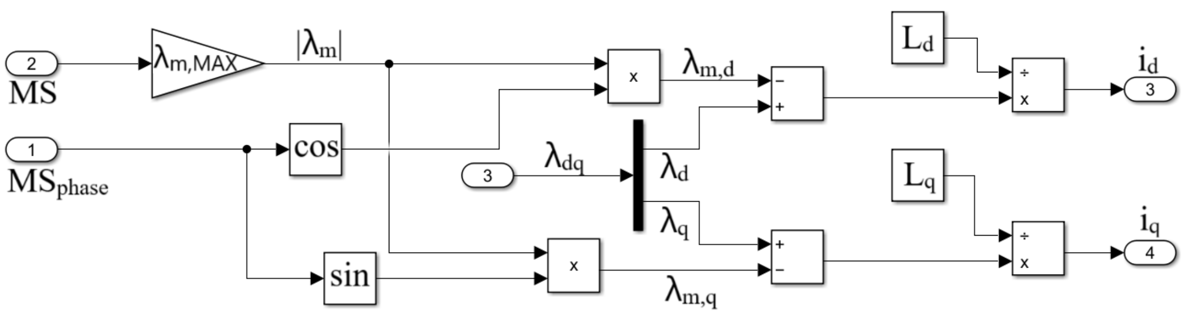

Figure 2.16: Inverse magnetic model with constant inductances

This solution can be adopted while maintaining good model accuracy, as the SPM rotor geometry and overall motor characteristics have minimal cross-coupling and saturation effects.

2.3.3 Maps-based magnetic model

A second refinement of the model involved reintroducing the flux maps, but this time specifically for the armature flux, while maintaining the previous formulation for the magnet flux. Allowing to manage a minor number of maps, while increasing the model accuracy.

The armature flux, is evalueted as:

$$\begin{cases} \lambda_d^L(i_d, i_q, MS) = \lambda_d - MS \cdot \lambda_{m,MAX} \cdot \cos\left(MS_{phase}\right) \\ \lambda_q^L(i_d, i_q, MS) = \lambda_q - MS \cdot \lambda_{m,MAX} \cdot \sin\left(MS_{phase}\right) \end{cases} \tag{20}$$

Then the armature flux values are input to the inverse armature flux, retrieving the i_{dq} currents.

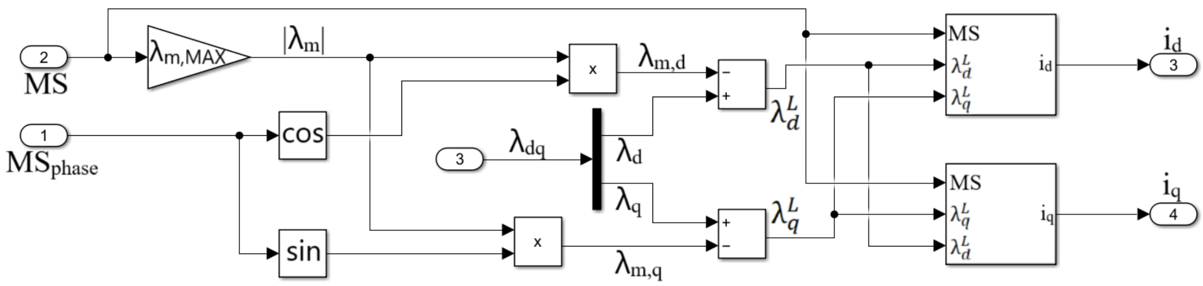

Figure 2.17: Maps-based magnetic model

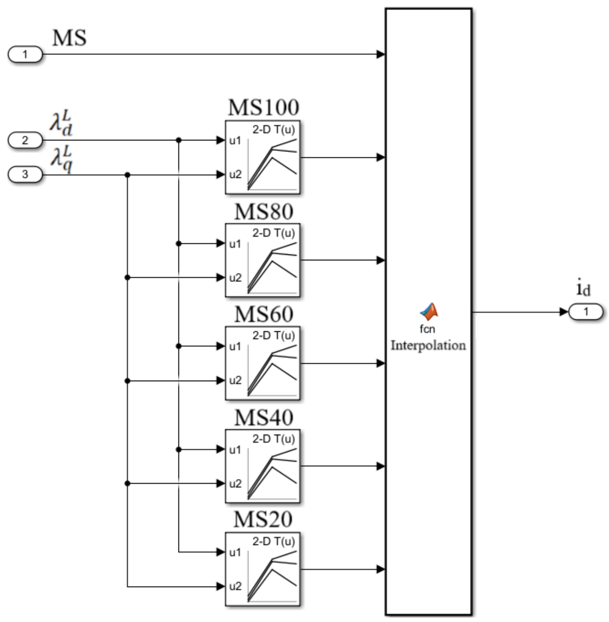

Figure 2.18: Armature flux maps model

As shown in Figure ∼2.18, the number of inverse flux maps, specifically the armature flux map, has been increased to cover 20%, 40%, 60%, 80%, and 100% of the MS values. This was achieved without imposing a significant computational burden, thanks to an interpolation algorithm that, using only the flux maps at 40% and 80% of MS, successfully generated the intermediate maps while considering only the case of uniform magnetization.
The flux characteristic generated from the interpolation algorithm are shown in Figure∼2.192.20.

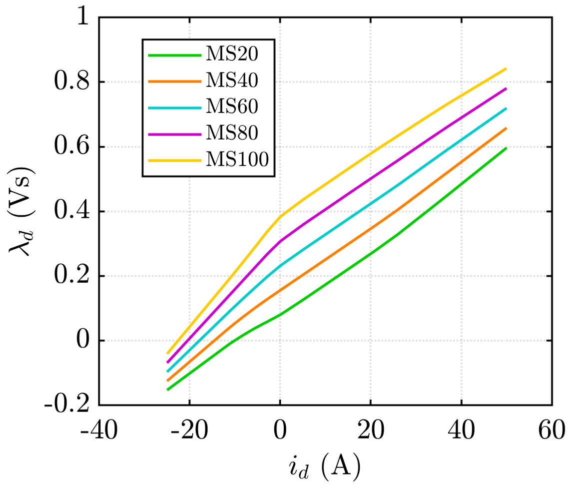

Figure 2.19: λ_d extended map

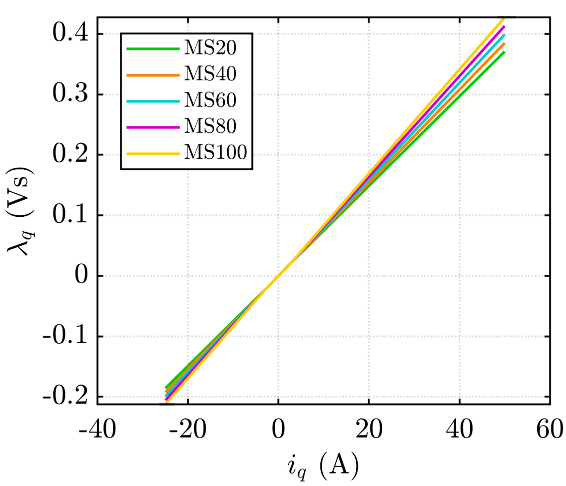

Figure 2.20: λ_q extended map

2.4 Comparison between the initial and the new models

The following section presents a comparison of the results obtained from the initial model and the new model. To highlight the capability of the new model compared to the initial one, has been decided to input two demagnetization current pulse on the same magnetization state isoline, in order to evaluate both cumulative and misalignment effects, in a single simulation.

The current pulse are represented in Figure~2.21, in the demagnetization plane, and the specific values for the first and second pulse are respectively: $i_d = -16.63A$, $i_q = 0A$ and $i_d = -19.19A$, $i_q = 23.62A$.

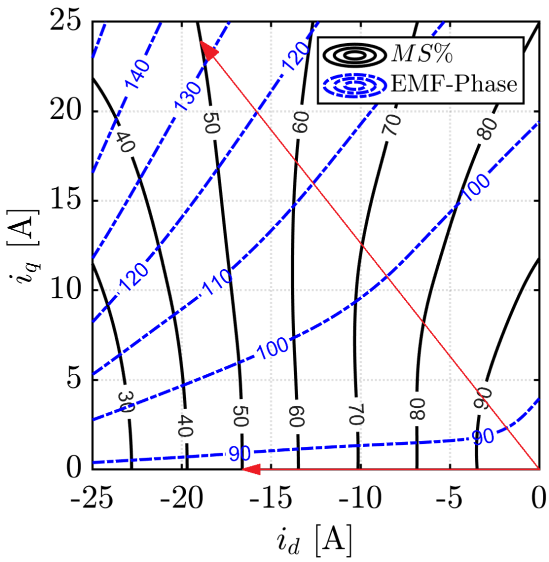

Figure 2.21: Current pulses in the demagnetization plane

For the new model simulation, only the maps-based approach was used, without repeating it for the L-Constant model. This is because the De-mag. and Re-mag. model remains the same for both, as the focus of this test is on their behavior. The results for the L-Constant model will be presented in the next chapter, where they will be compared to the FEA model for validation.

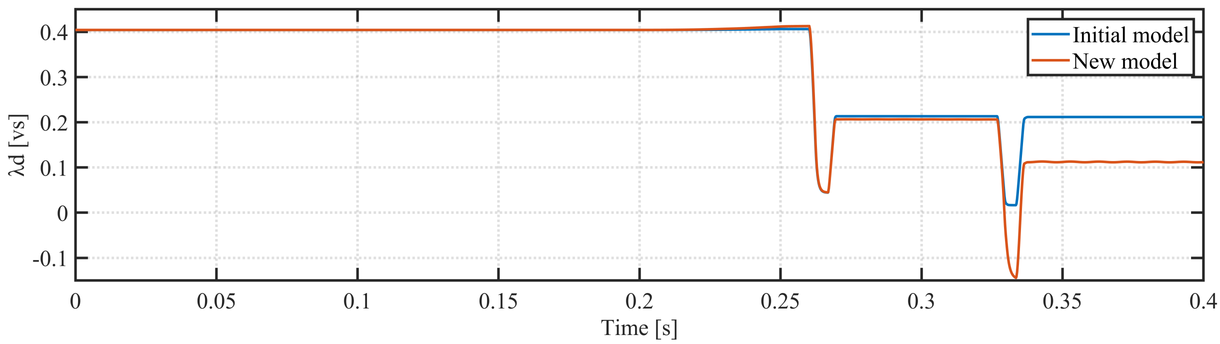

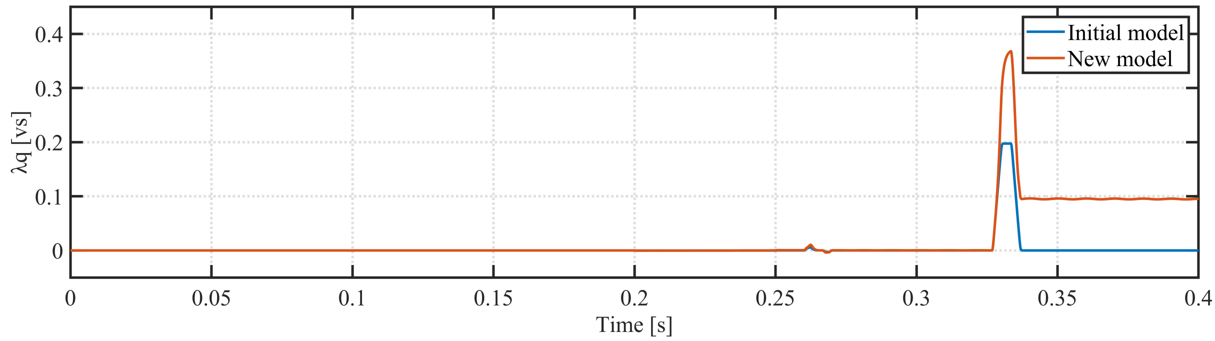

Figure 2.22: λ_{dq} flux linkage - model comparison

While after the first pulse the fluxes, in their respective axis, remains equals between the initial and the new model, after the second pulse the values diverge completely.

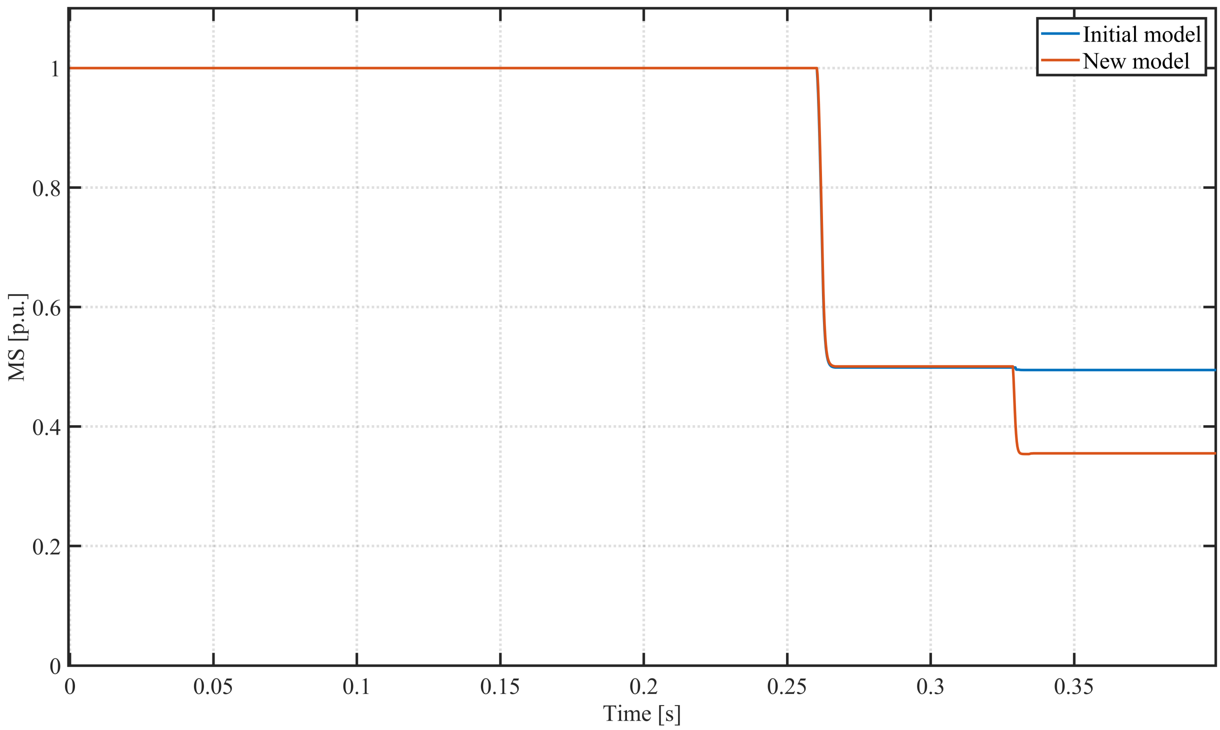

Figure 2.23: Magnetization state-model comparison

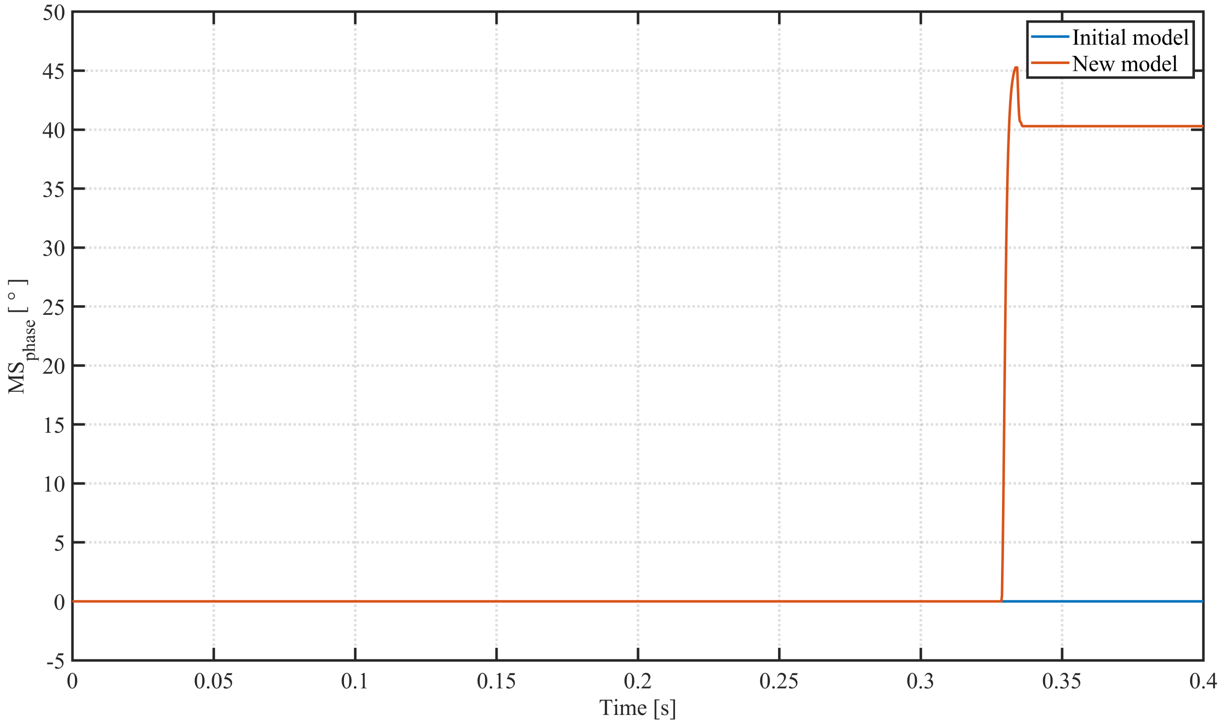

Figure 2.24: Magnetization state phase-model comparison

As seen, the old model cannot account for misalignment effect and the cumulative effect that can result from it, it can only account cumulative effect in case of symmetrical magnetization . As previously mentioned, when two pulses are applied to the same isoline, the old model shows no significant change in the MS. A slight change is observed, but this is due to the Simulink environment, where currents are provided as references to the control system. As a result, the actual currents reaching the motors are slightly different. Proof that the results of the new model are correct will be provided in the next chapter through a comparison with the FEA model.

3 Comparison between Simulink and Jmag F.E. models

This chapter presents a comparative analysis between the results obtained from the Finite Element analysis simulation and the Simulink model developed for this study, with the objective of validate the developed model, evaluating it's accuracy and reliability.

The FEA software chosen for those analysis is Jmag. Jmag is a simulation software,developed by JSOL Corporation, created to analyze and design electrical devices, such as motors, actuators and circuit components.

This software in particular has been selected due to its capability in performing analyses involving variable magnetization phenomenon, and the possibility to include in the simulation supply circuits, making it possible to incorporate power electronics into the analysis.

For simulating the dynamic behavior of electrical machine Jmag, offer two solutions: Jmag Designer and Jmag-RT. Jmag Designer is the core tool of the software, being the actual FEA software that also allows to simulate different drive conditions. While Jmag-RT generates systems models based on the finite element model results, resulting very similar to the Simulink environment used in this work. Being the objective the validation of the created model the choice fell on the actual FEA model, being the most accurate.

To focus solely on the motor model while minimizing the influence of the control code required for running the simulation in the Simulink environment, has been decided to perform the simulation in JMAG using three piloted current generators, one for each phase. These generators directly supply current in the abc reference frame, rather than converting it from the dq reference frame. By doing so, the current computed by the Simulink model is directly applied to the JMAG model, ensuring consistency between the two. This approach allows for a more precise evaluation of the motor model characteristics, focusing particularly the flux and the magnetization state. These two factors are crucial, as they directly impact the accuracy of the model and its ability to faithfully represent the motor's electromagnetic behavior.

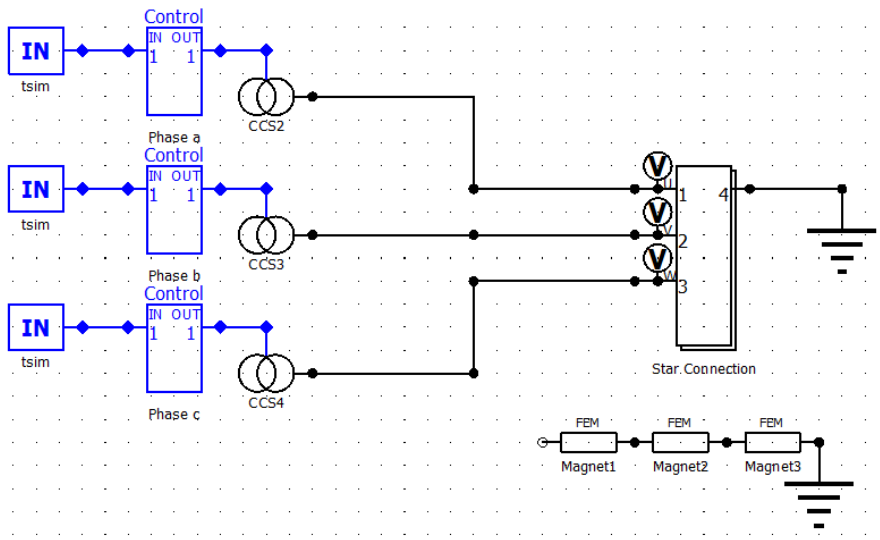

Figure 3.1: Circuital representation inside Jmag

Every simulation begins with the permanent magnets fully magnetized, as required by JMAG constraints. Therefore, when conducting a test that involves remagnetization, it is first necessary to demagnetize the magnets.

For each simulation, the motor is externally driven to rotate according to the same speed reference, shown in Figure~ 3.2, ensuring consistency across all test conditions.

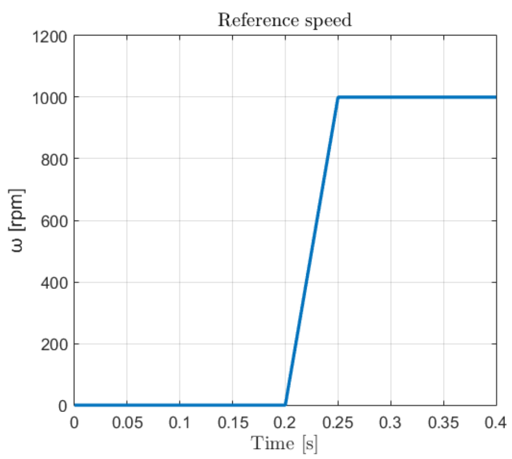

Figure 3.2: Speed reference

Although the models were developed sequentially, first validating the constant inductance model before creating the one with inverse armature flux maps, it was decided to combine both models in a single comparison for each test. This approach minimizes redundancy and avoids an excessive number of graphs, which could lead to confusion.

3.1 Open circuit test

The first test conducted is the open circuit test, where the machine is rotated without supplying power to the phases. This test is conducted to ensure that the models have identical initial conditions and to assess the impact of the neglected phenomena within them.

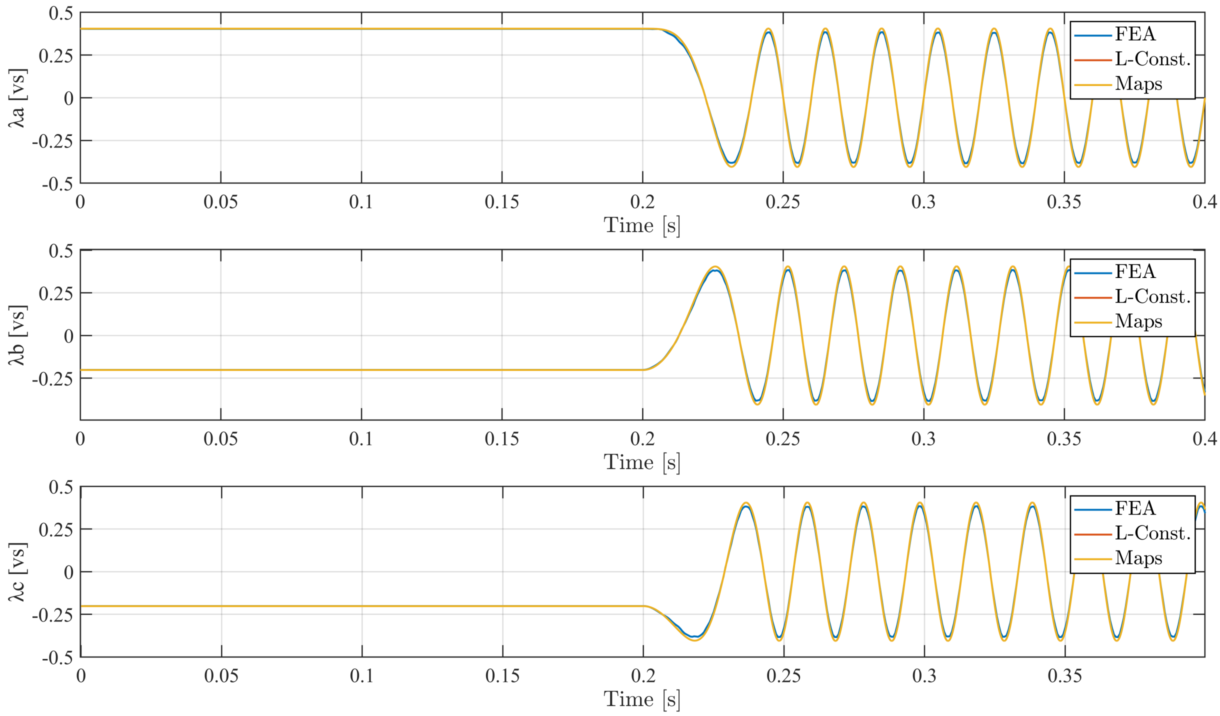

Figure 3.3: Flux linkage in *abc* reference frame-open circuit test

All three model begin at standstill under the identical conditions. However, as the motor starts spinning, slight discrepancies emerge emerge between the flux in the FEA model and the Simulink models.

This difference arises because Jmag accounts for eddy currents induced in the magnets during rotation, according to Lenz's law, these eddy currents generate opposing magnetic fields that partially shield the magnets, leading to a slight reduction in overall flux. While this effect is small, it remains noticeable, simplified analytical models like the ones in Simulink do not consider eddy currents, which explains the observed discrepancy.

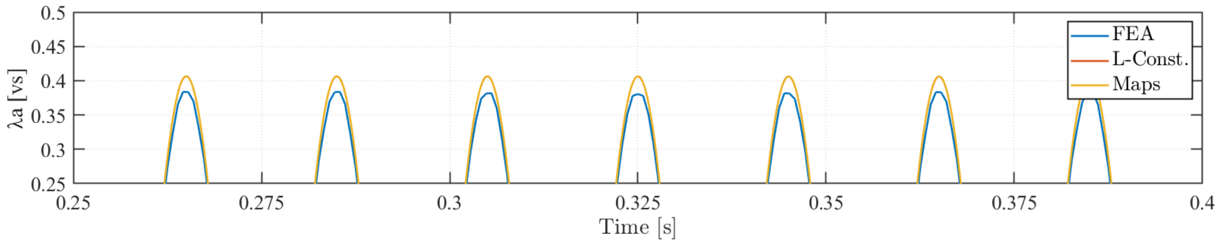

Figure 3.4: Close-up of λ_a-open circuit test

In order to better quantify the error, the flux components are transformed into the dq reference frame, error that settles around the 5% in the d-axis, while in every case the q-axis is null.

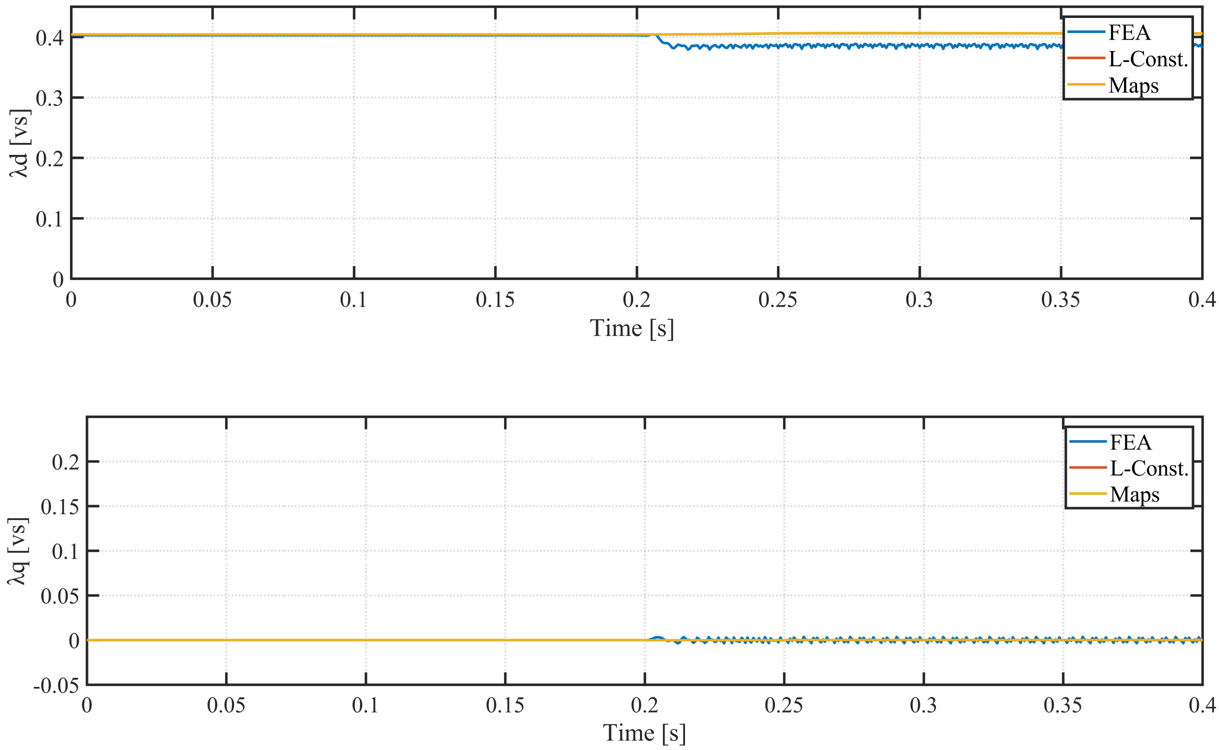

Figure 3.5: Flux linkage in dq reference frame-open circuit test

The analysis of the flux linkage in the dq reference frame also allows to highlight another phenomenon neglected in the Simulink models, but present in the FEA one, the spatial harmonics. Spatial harmonics are variations in the magnetic field distribution within an electric machine caused by non-idealities in the physical structure, that instead of producing a purely sinusoidal air-gap flux introduce higher-order harmonic components in space, causing the small ripple noticeable in the Figure~3.5.

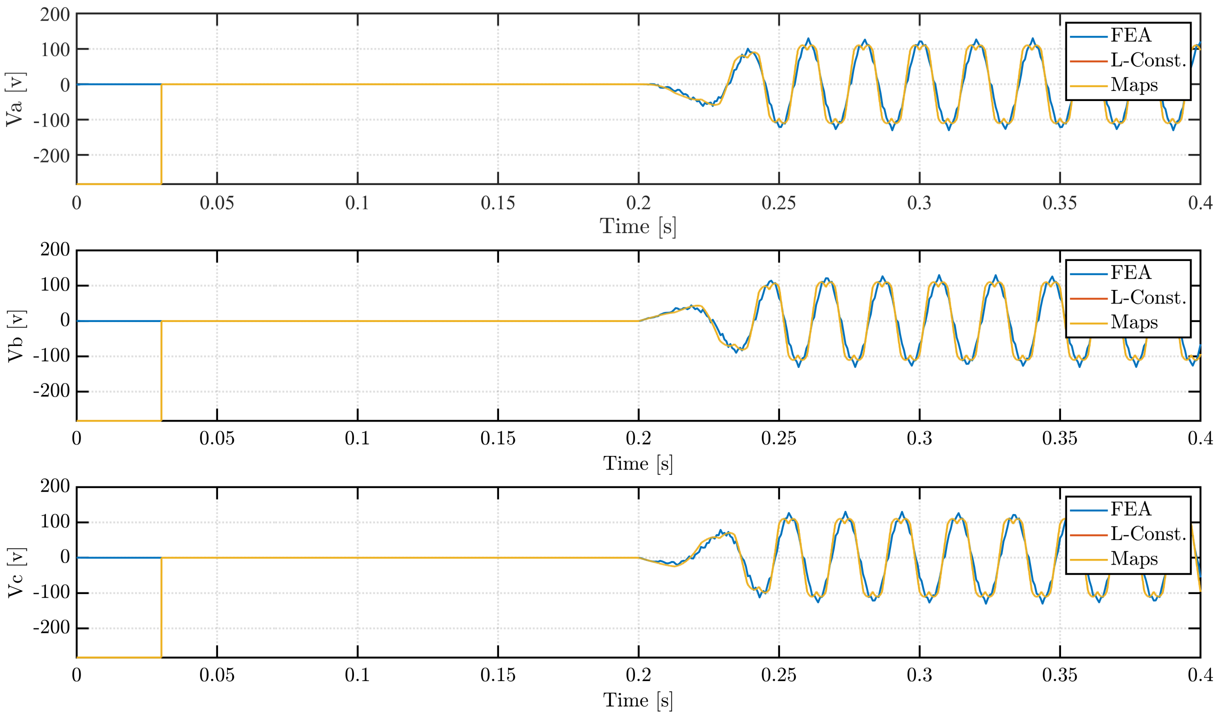

Figure 3.6: Voltage abc-open circuit test

3.2 De-magnetization tests

To test the model under Demagnetization conditions, has been decided to firstly perform a demagnetization using a d-axis only current pulse, than to perform another test to assess the capability of representing the uneven demagnetization. The chosen current pulses are shown in Figure∼3.8.

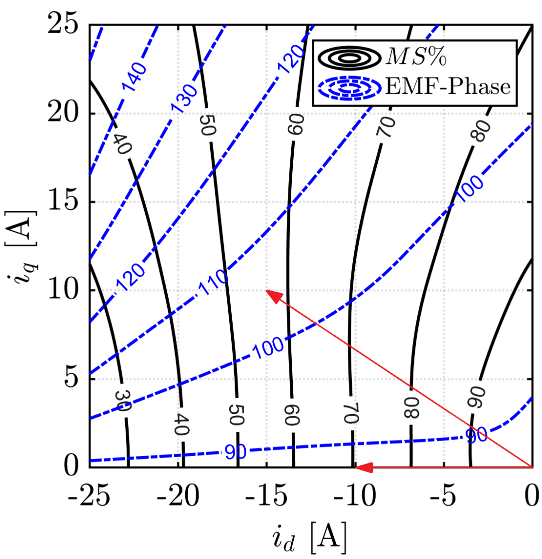

Figure 3.7: De-mag. pulses used for the tests

3.2.1 d-axis Demagnetization

The first demagnetization test consist in a current pulse along the d-axis ($i_d = -10A, i_q = 0A$).

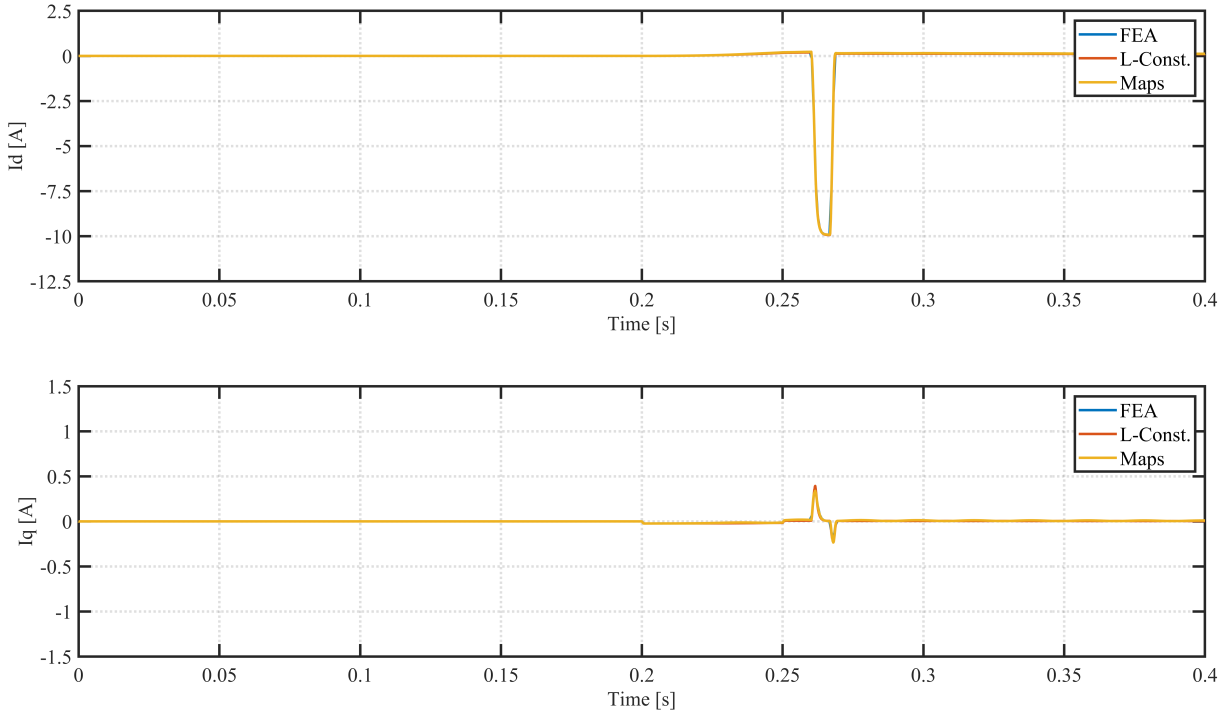

Figure 3.8: De-mag. pulses in the dq reference frame

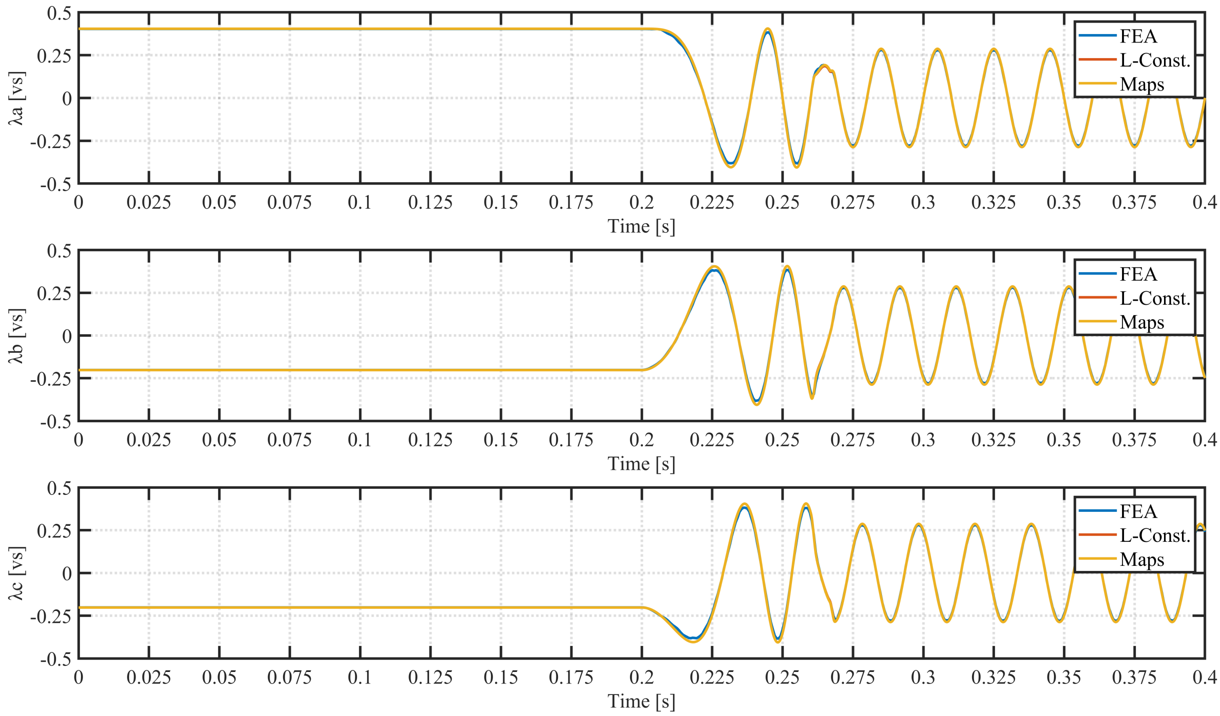

Figure 3.9: Flux linkage in abc-De-mag. in d-axis

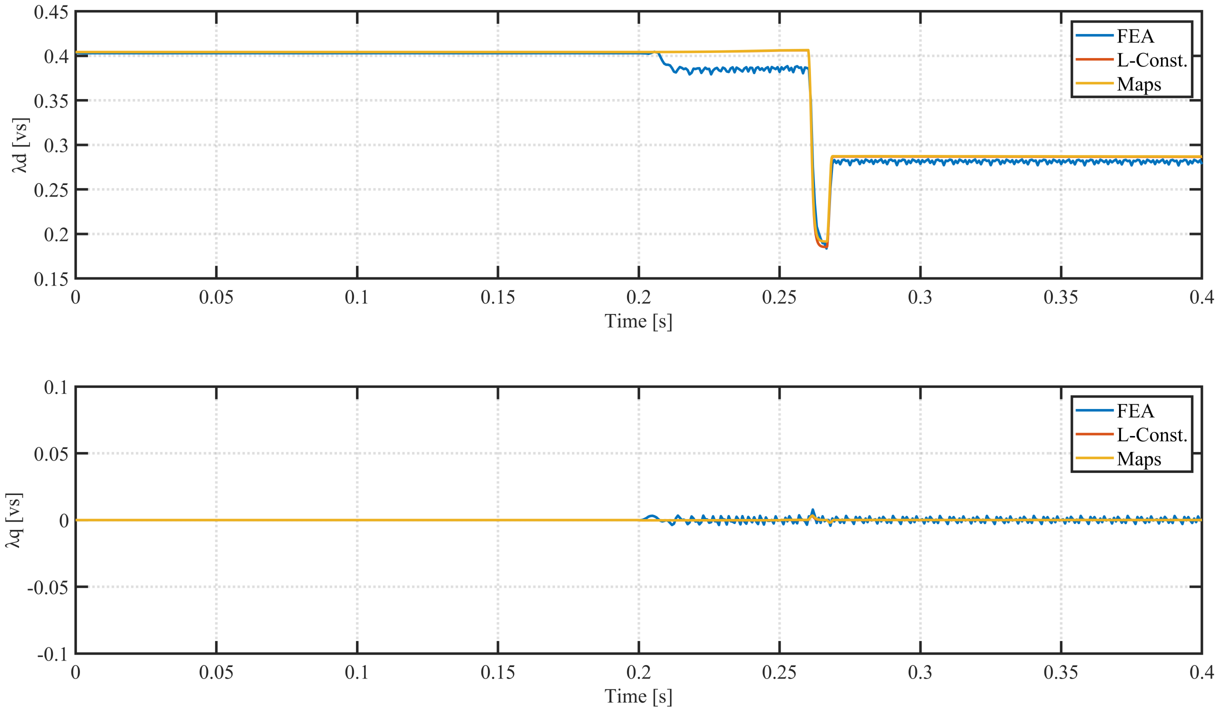

Figure 3.10: Flux linkage in dq-De-mag. in d-axis

Although it may seem larger than the open circuit test, the difference between the fluxes on the d-axis when the motor starts to rotate is always around 5%, decreasing further after demagnetization to around 2.5%.

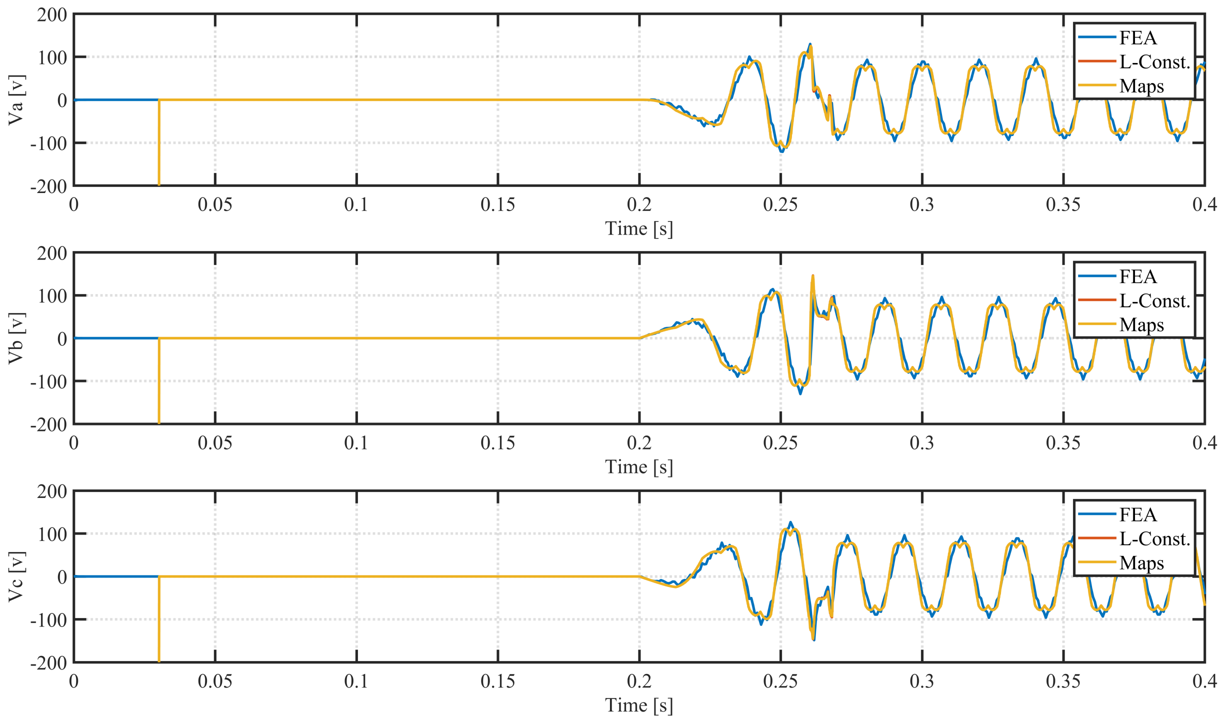

Figure 3.11: Voltage in abc-De-mag. in d-axis

3.2.2 Second quadrant Demagnetization

The second demagnetization test consist in a pulse in both d and q-axis in order to unevenly demagnetize the PMs $(i_d = -15A, i_q = 10A)$.

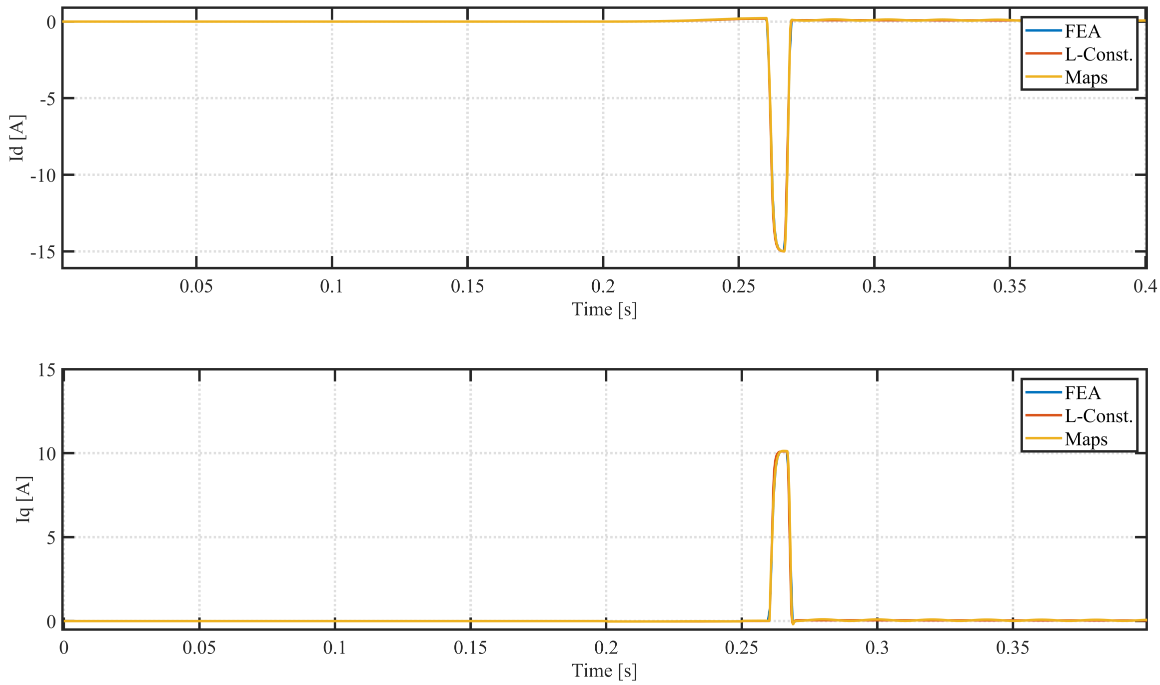

Figure 3.12: Current in dq-De-mag. in dq-axis

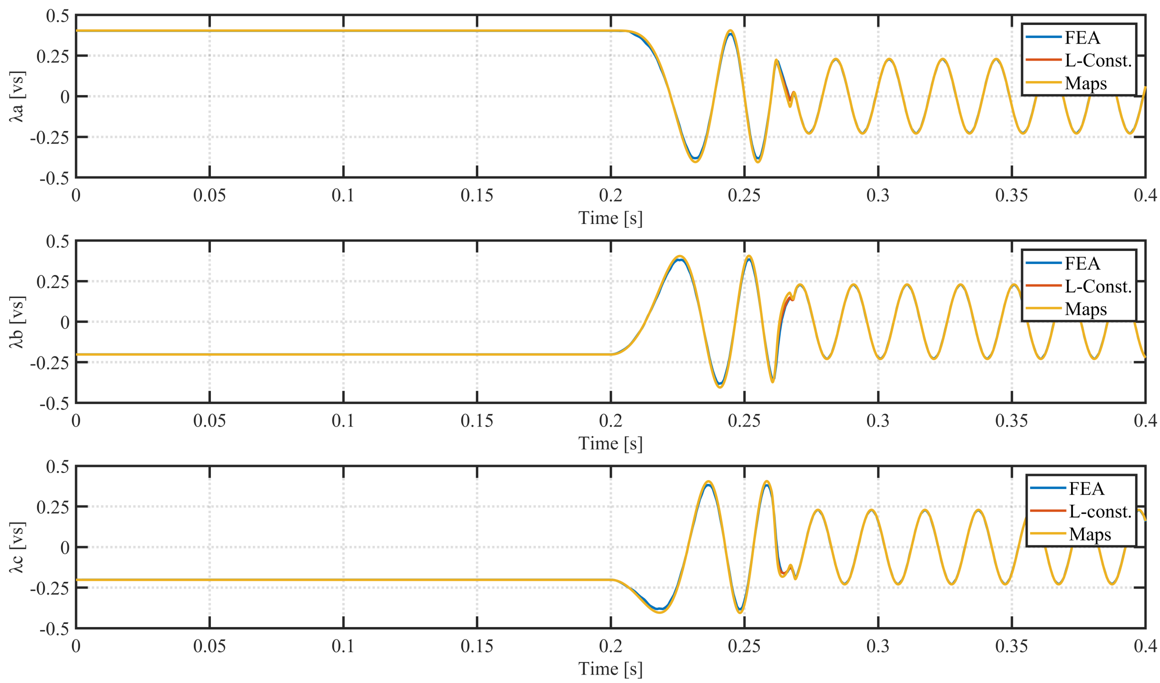

Figure 3.13: Flux linkage in abc-De-mag. in dq-axis

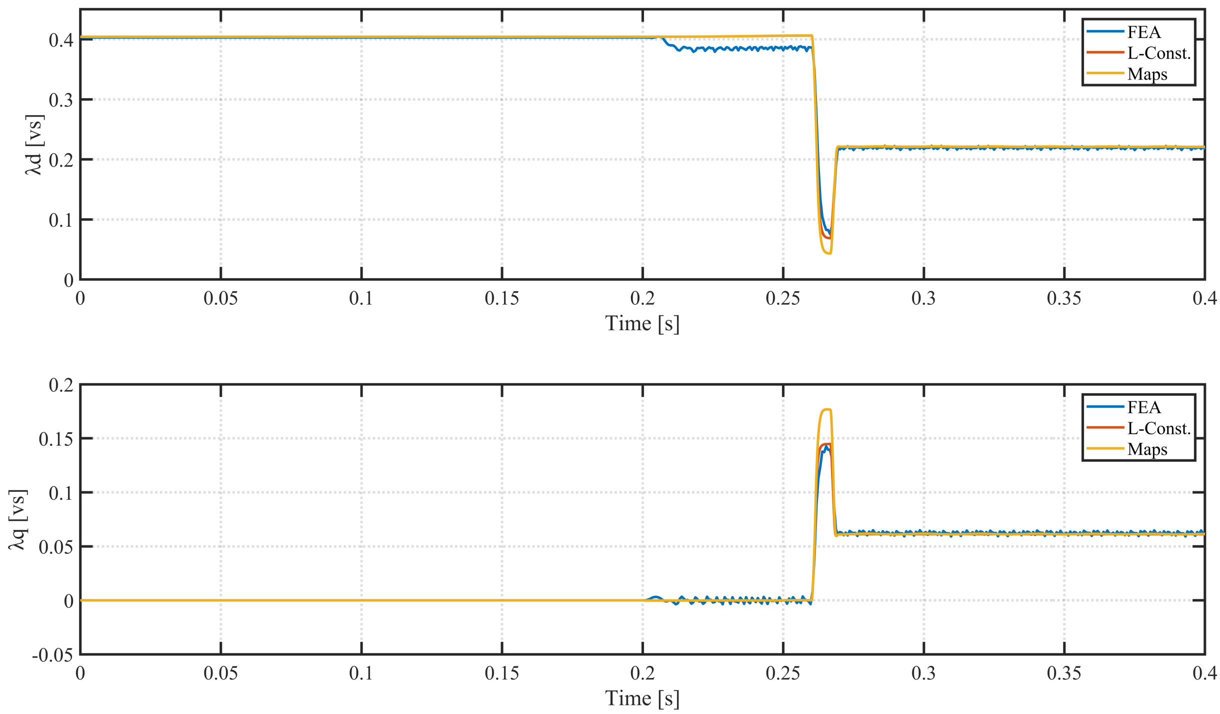

Figure 3.14: Flux in dq-De-mag. in dq-axis

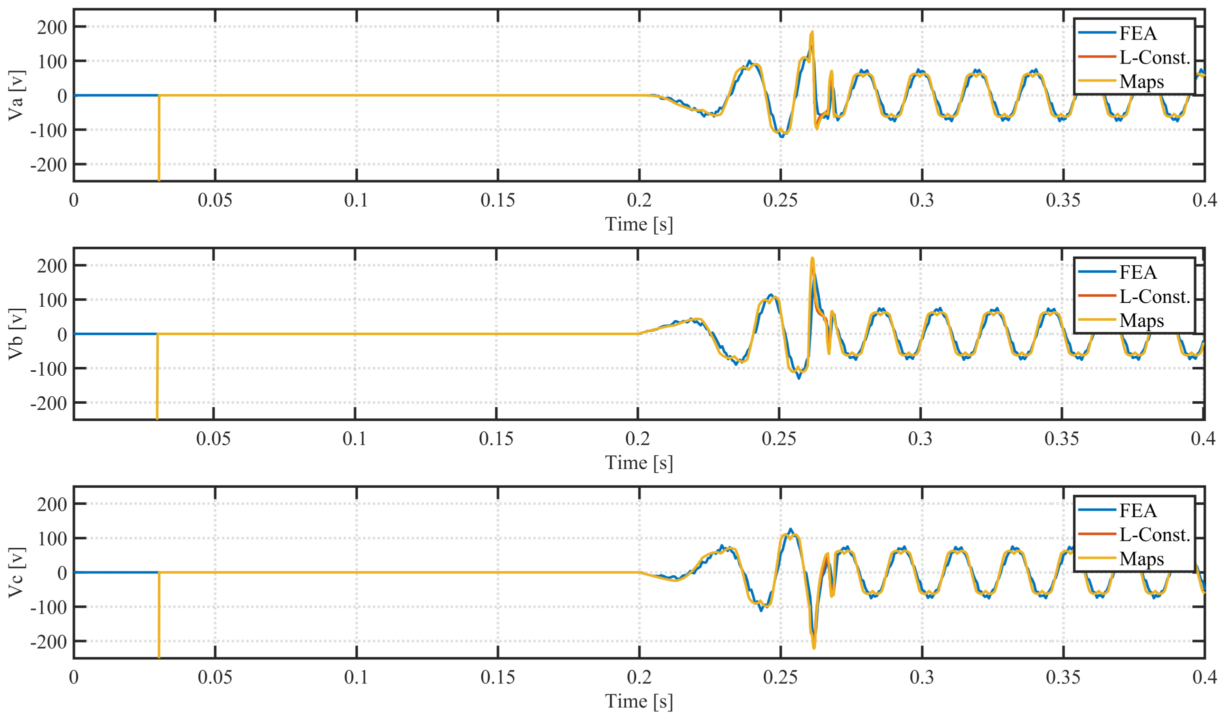

Figure 3.15: Voltage in abc-De-mag. in dq-axis

3.3 Re-magagnetization tests

As previously mentioned, due to JMAG constraints, each simulation must begin with the PMs fully magnetized. Therefore, for the remagnetization test, an initial demagnetization pulse is required before proceeding with the remagnetization process. In both Simulink models, any condition within the magnetization maps can be used as a starting point, making the demagnetization step unnecessary. However, for consistency with the test procedure, the same current will be applied. The chosen current pulses are shown in Figure ~3.16,3.17.

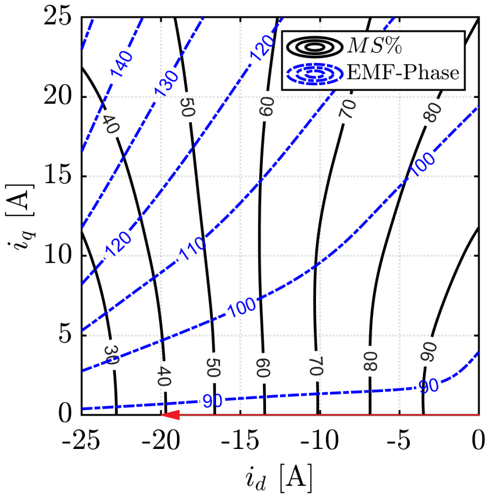

Figure 3.16: Demag. pulses

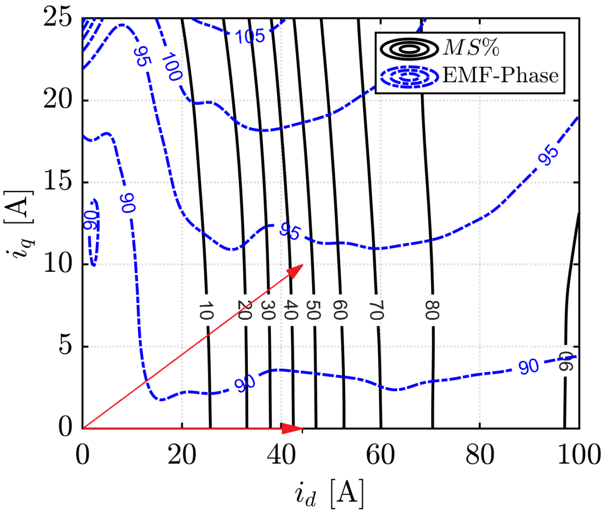

Figure 3.17: Re-mag. pulses

3.3.1 d-axis Remagnetization

The first Remagnetization test consist in a first demagnetization current pulse along the d-axis $(i_d = -20A, i_q = 0A)$, than after that the remagnetization pulse is applied also, only, along the d-axis$(i_d = 45A, i_q = 0A)$.

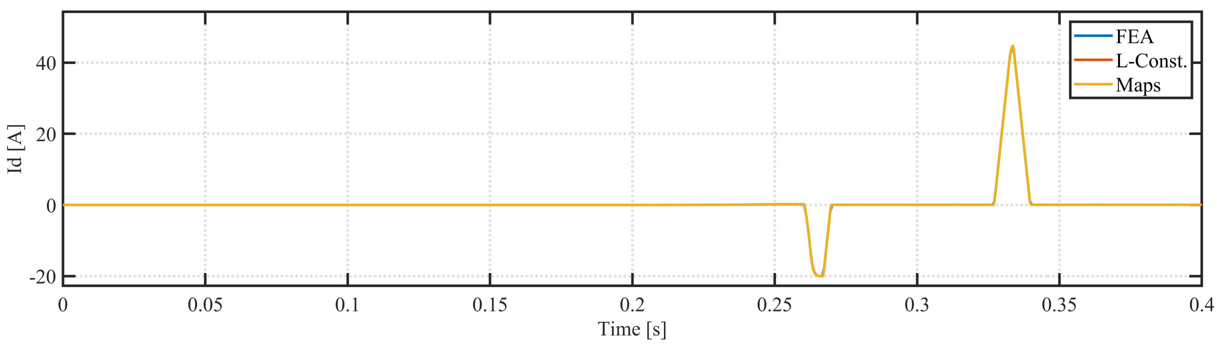

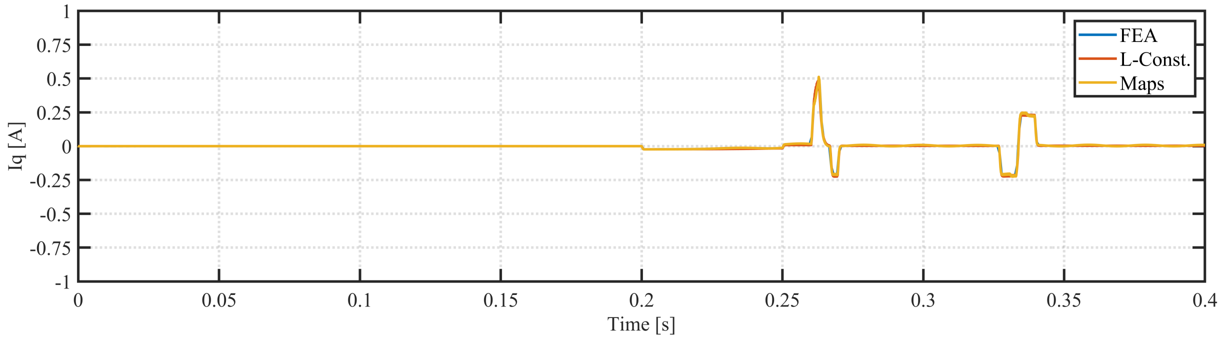

Figure 3.18: Current in dq-Re-mag. in d-axis

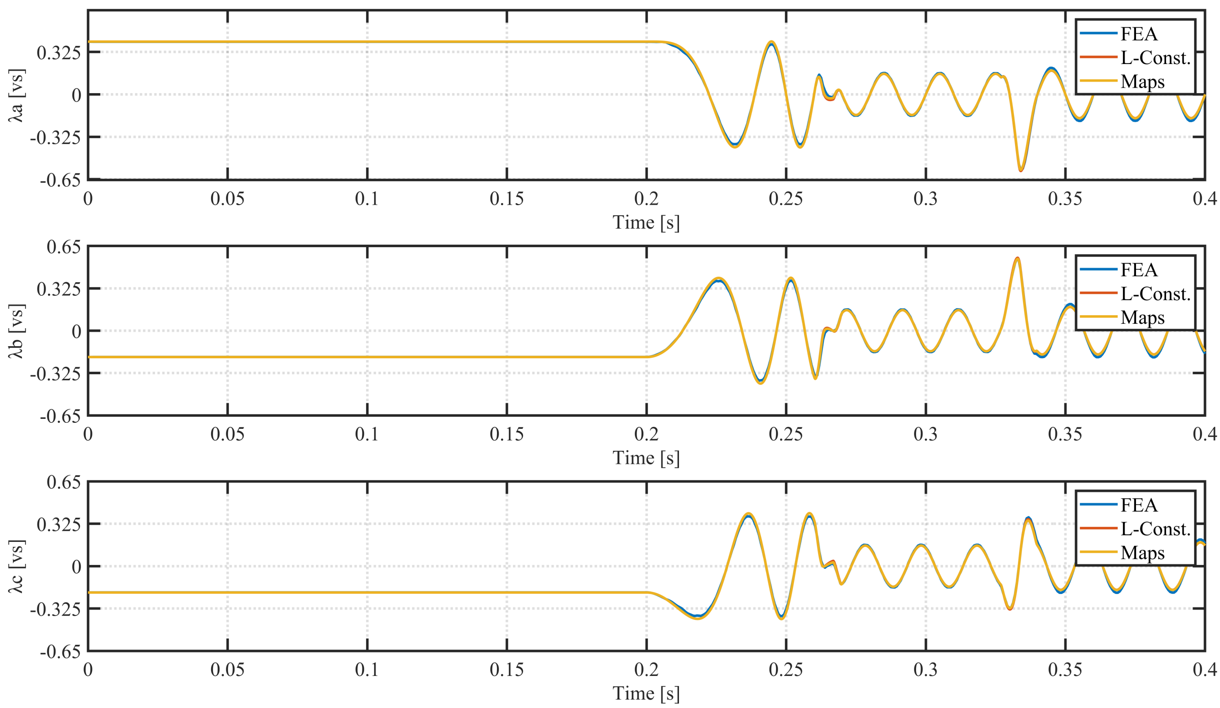

Figure 3.19: Flux linkage in abc-Re-mag. in d-axis

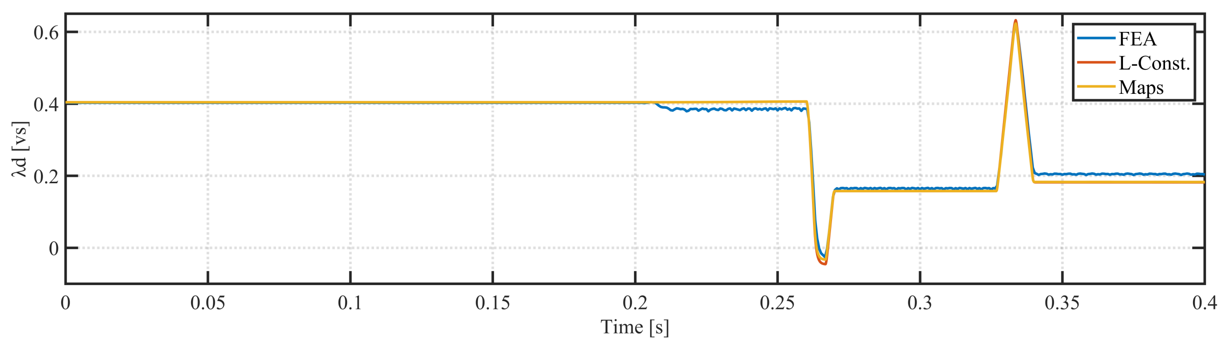

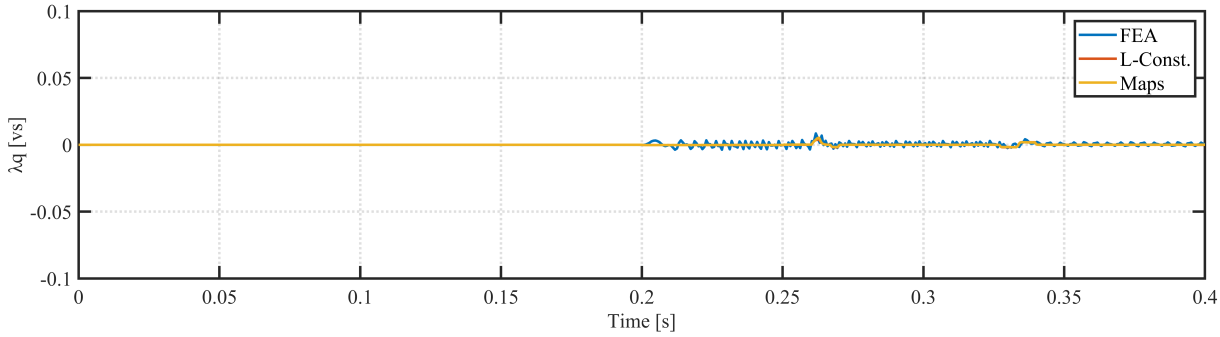

Figure 3.20: Flux in dq-Re-mag. in d-axis

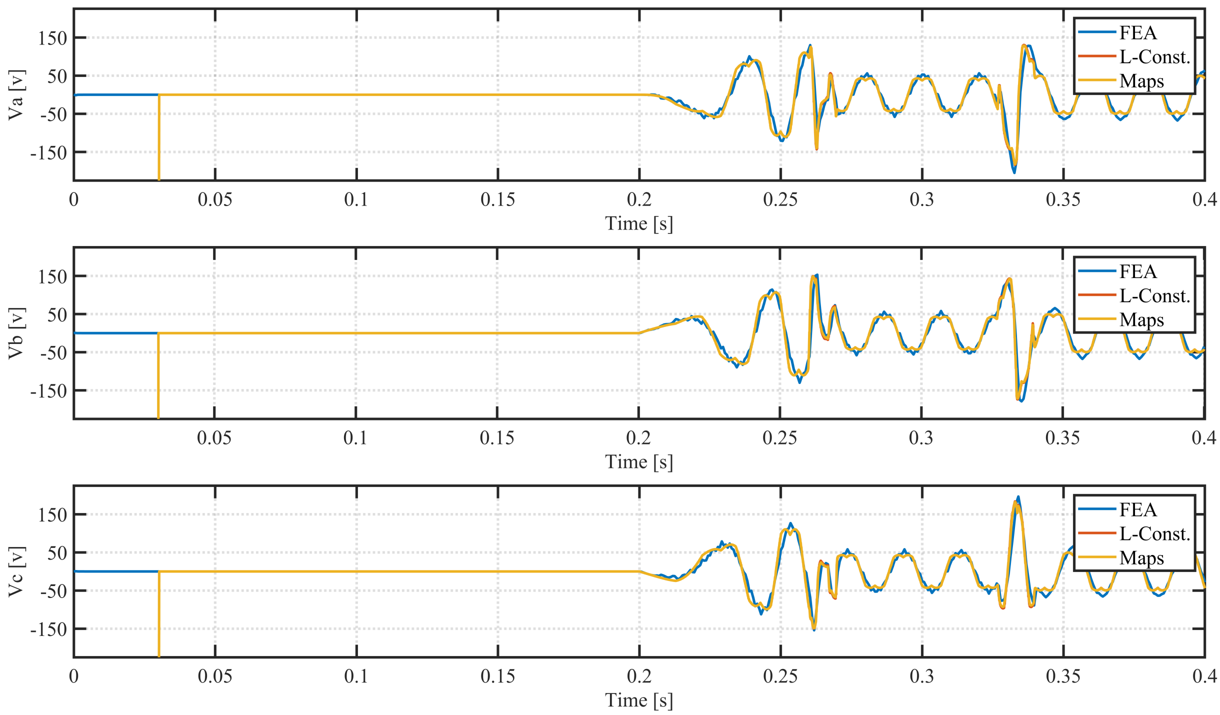

Figure 3.21: Voltage in abc-Re-mag. in d-axis

3.3.2 First quadrant Remagnetization

In the second test the same demagnetization current pulse is applied, but this time the remagnetization pulse has also a component in the q-axis $(i_d = 45A, i_q = 10A)$.

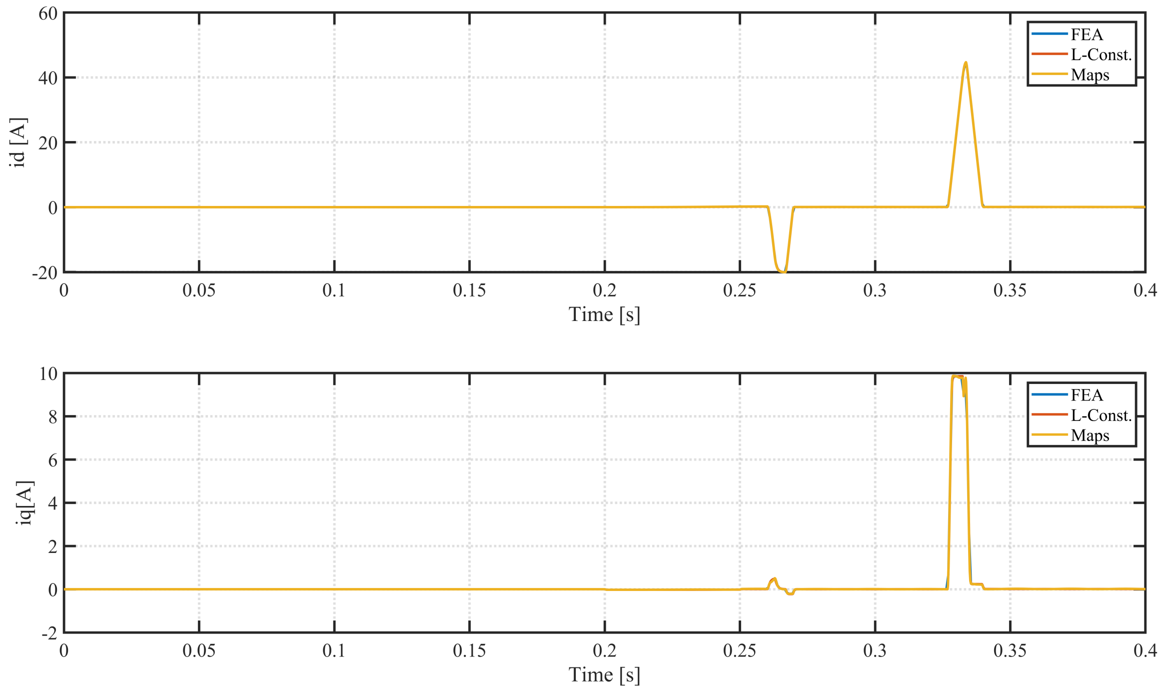

Figure 3.22: Current in dq-Re-mag. in dq-axis

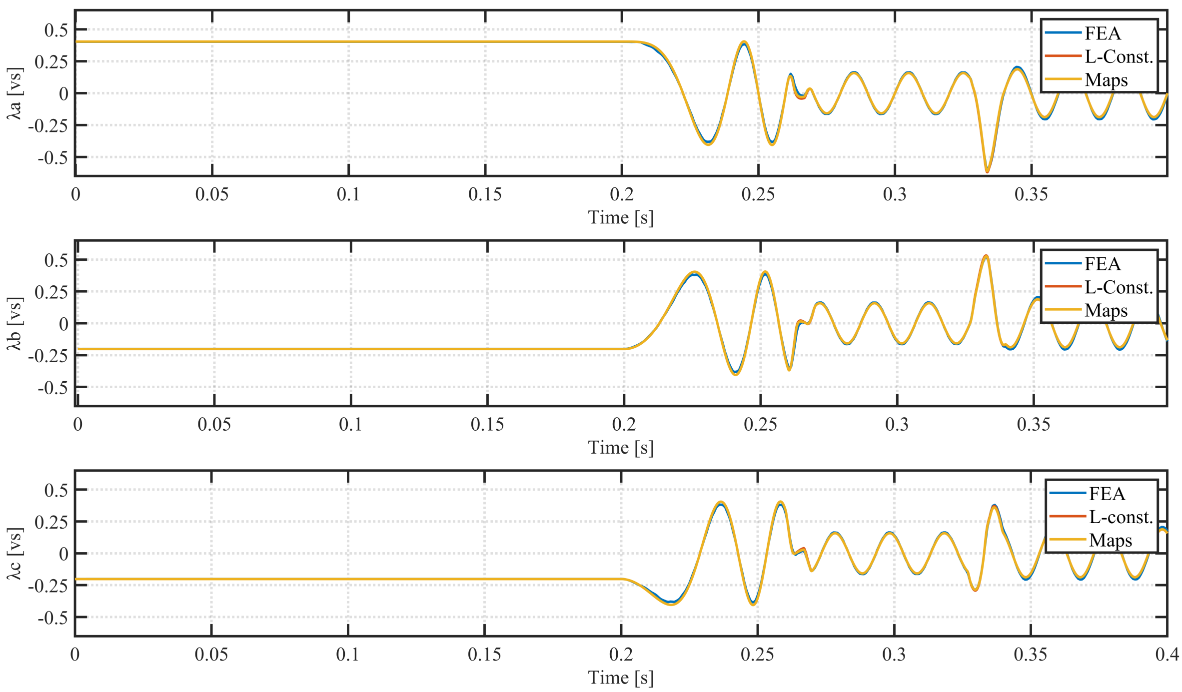

Figure 3.23: Flux linkage in abc-Re-mag. in dq-axis

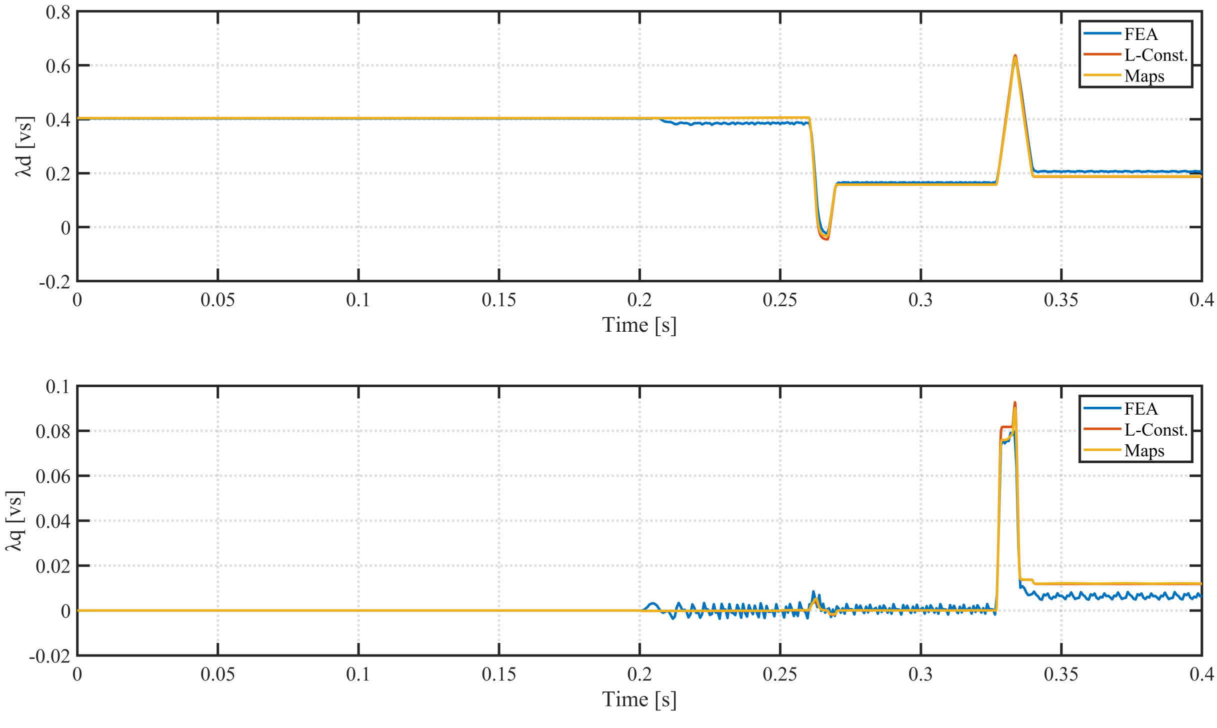

Figure 3.24: Flux in dq-Re-mag. in dq-axis

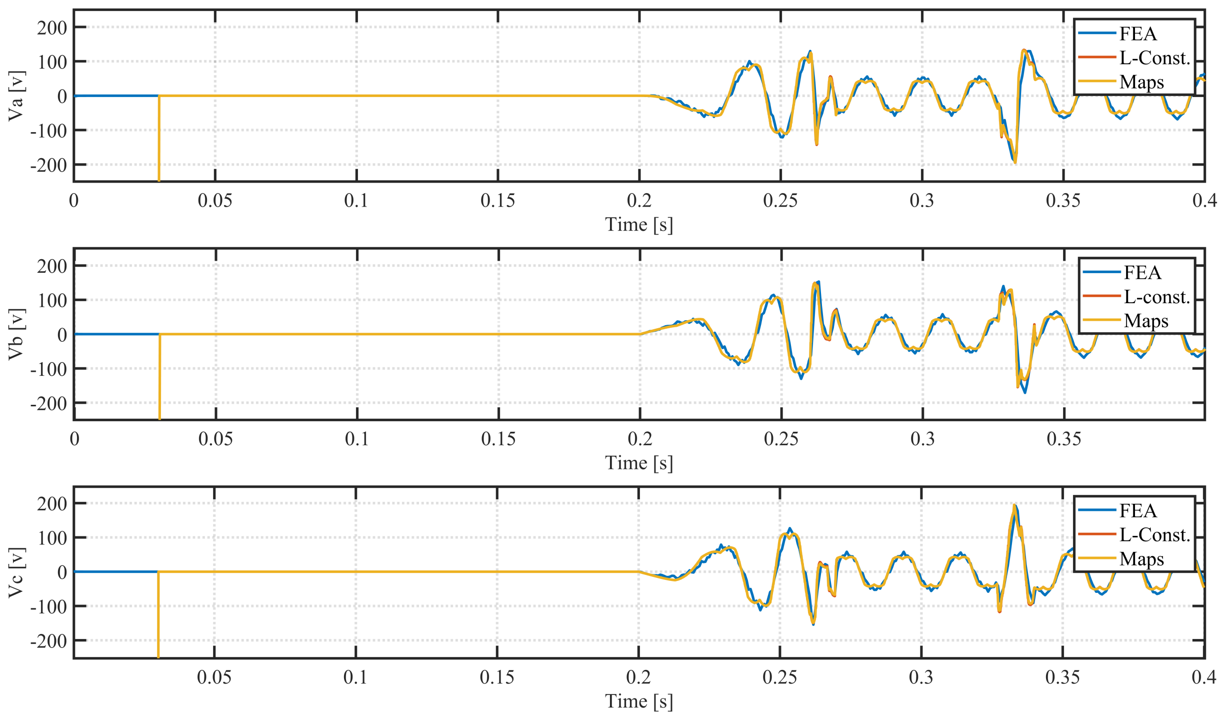

Figure 3.25: Voltage in abc-Re-mag. in dq-axis

3.4 Cumulative effect test

The final test replicates the one conducted to compare the initial Simulink model with the new one, aiming to verify whether the results of the new model are indeed accurate. The current pulses used are the same as those previously shown in Figure∼2.21, summarized as follows: $i_d = -16.63A$, $i_q = 0A$ and $i_d = -19.19A$, $i_q = 23.62A$, for the first and second pulse respectively.

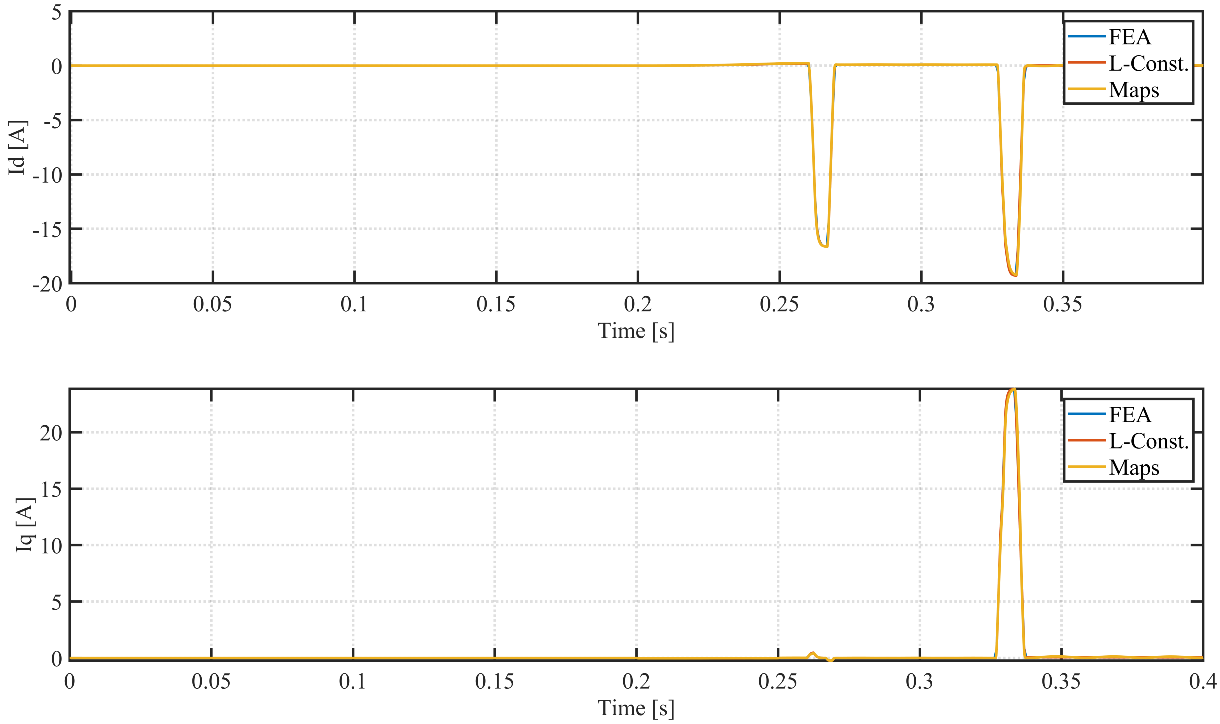

Figure 3.26: Current in dq reference frame-Cumulative effect test

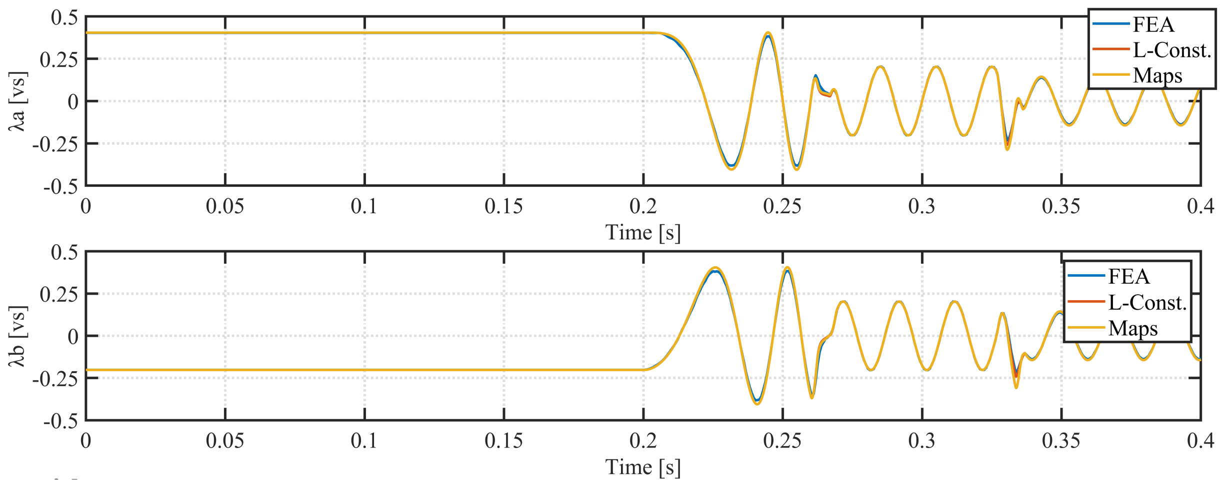

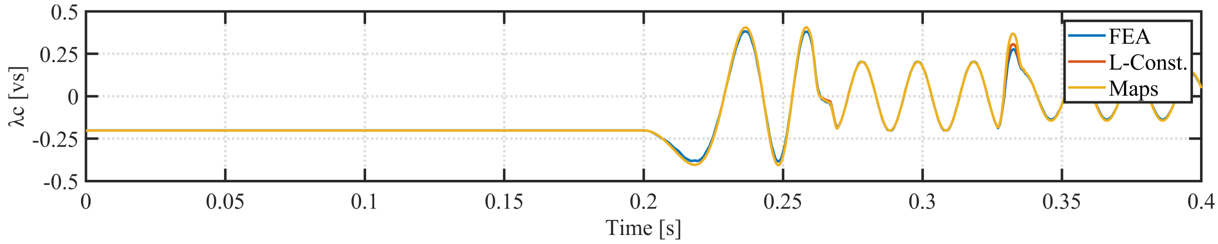

Figure 3.27: Fluxes in abc reference frame-Cumulative effect test

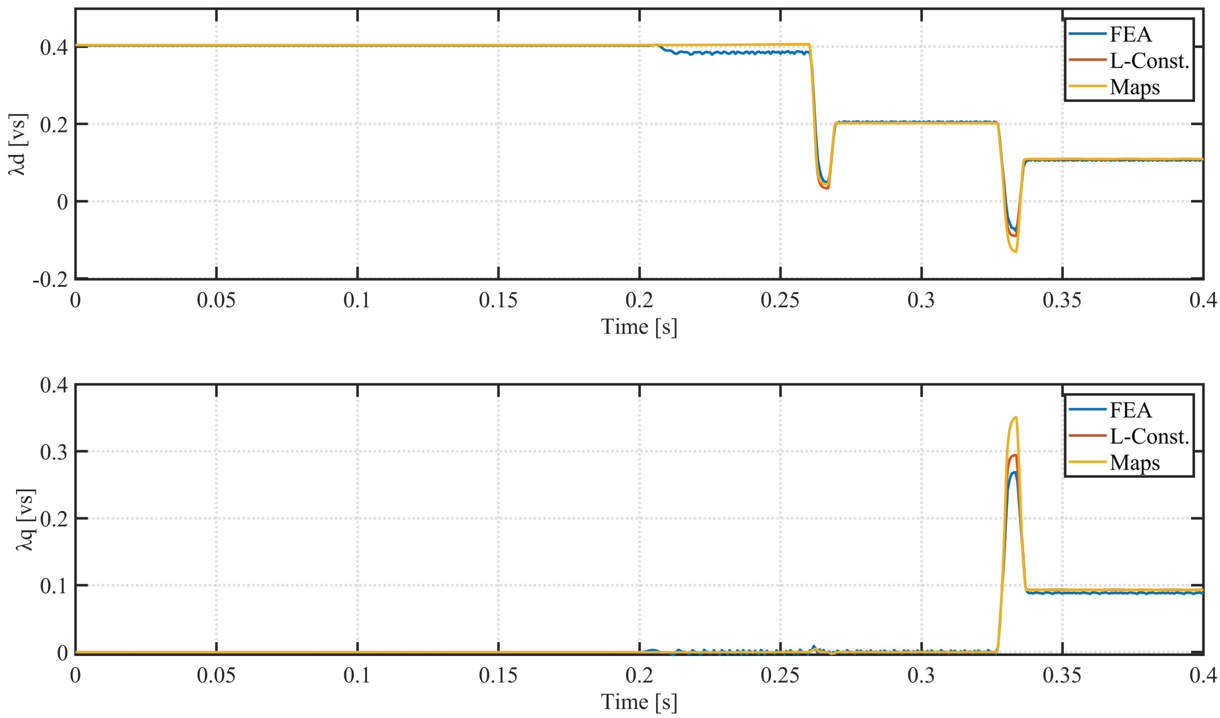

Figure 3.28: fluxes in dq reference frame-Cumulative effect test

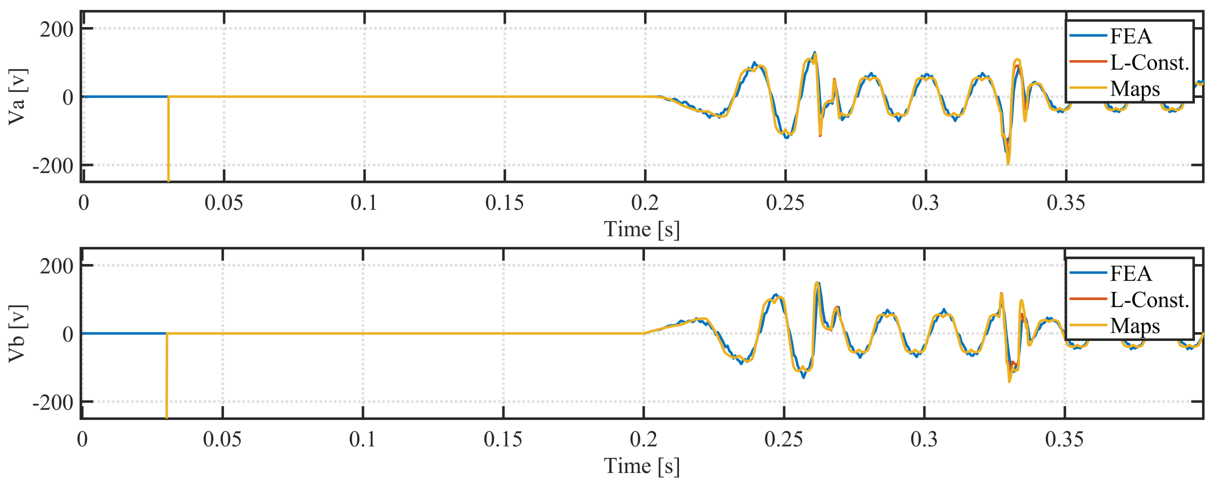

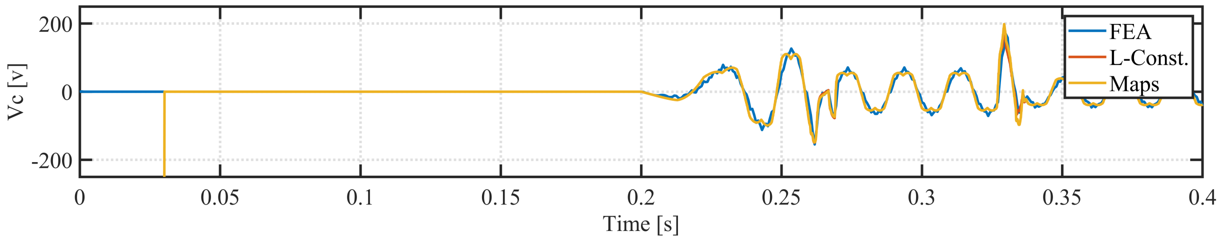

Figure 3.29: Voltage in *abc* reference frame-Cumulative effect test

3.4.1 Comments on comparison results

The results from the different tests are positive, confirming that both Simulink models accurately represent the motor's behavior. While there is room for improvement, the discrepancies remain within a reasonable 5% range. Given that the primary objective of the model is to balance accuracy with computational effort for control strategy studies, these results demonstrate that it is a sufficiently precise yet fast-executing solution, further highlighted by the model's execution time of just 7 seconds for a 0.4s simulation, compared to the 10 to 15 minutes required for FEA analysis.

4 Motor control for the VF-PMSM

This chapter explores the control strategies for the Variable Flux Permanent Magnet Synchronous Motor. In particular it focuses on the development of and adequate observer, able to correctly observe the flux but also to estimate the magnetization state and its phase. Further more a modified version of a field oriented current control is developed, that take advantage of the estimated MS_{phase} to compensate the misalignment of the reference system, avoiding the possible harmful consequences, such as: incorrect axis decoupling and to online MTPA tracking for the sake of better efficiency.

4.1 Digital control generalities

As mentioned before, in chapter two, one of the core blocks of the simulation environment is the digital control block, representing the microcontroller. The working principle is the same as for a real microcontroller, a trigger mechanism initiates the execution of the Motor Control code at a constant sampling rate, mimicking the IRS call, mandatory to guarantee the real time operation.

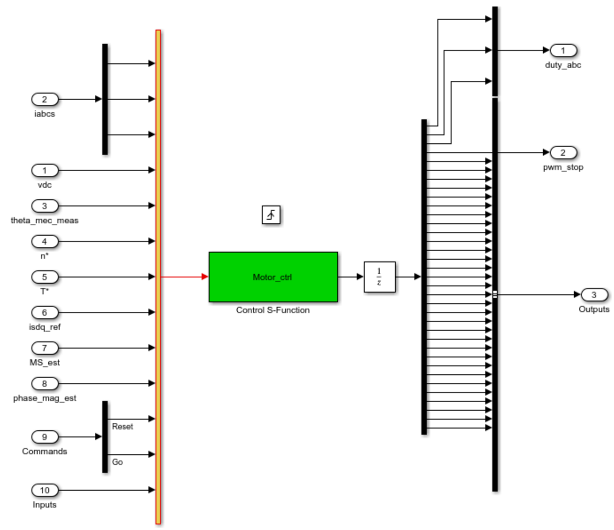

Figure 4.1: Digital control block

Also the inputs and outputs are actually managed as if they were actually interfaced with a microcontroller, making the model very similar to the scenario of a real control system. Even a delay block is added to simulate the actual latency in the operation of a real control system.

Following the same realistic logic, the control code is organized as a real one. Consisting of a series of different files, divided in to: Headers files which contains the constant, variables, macros and C functions declarations shared between the Source files which contains the actual motor control code and the used functions.

The interrupt service routine an by so the actual control code, is divided in, at least four, operating state or machine state. States that the system must pass through before it can actually start operating the electric machine, to guarantee a safe and correct operation of the system.

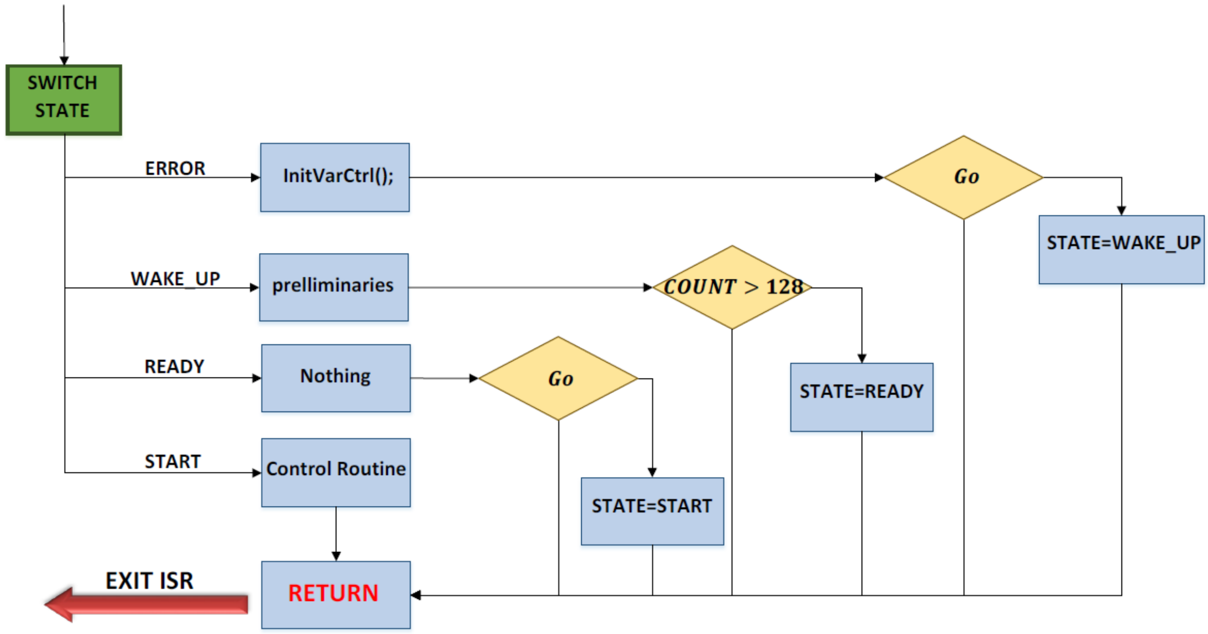

Figure 4.2: Machine state flow chart

The Error State is the default conditions at the systems startup or upon a reset, i a safety condition where the modulation is set to zero, and is mostly used to initialize variables.

Wake up state, it activate upon an external signal, activate the modulation, is used for preliminary operation such as offset computation, pre-load of the boot-strap capacitors, commissioning procedure and so on. Is a temporary state, meaning that upon a predetermined period of time it automatically move to the successive state.

Ready state, it communicate that the previous operation were successful and that the drive, upon receiving a GO signal, is prepared to start.

Start state, is the state were the drives actually work, following the control code instructions.

4.2 Field Oriented Control

Field oriented control is an advanced motor control technique used to achieve high-performance operation, that has become a standard in modern electrical drives application. Unlike traditional scalar control methods, which regulate voltage and frequency proportionally, FOC provides precise and independent control of torque and flux, similar to how a DC motor operates.

FOC by transposing the stator current from the abc stationary reference frame, to the dq rotational reference frame allows to see the currents as DC components. This transformation enables the decoupling of torque-producing current I_q from the and flux-producing current I_d, allowing for fast dynamic response, improved efficiency.

The general scheme of the Field Oriented Control is shown in Figure~4.3.

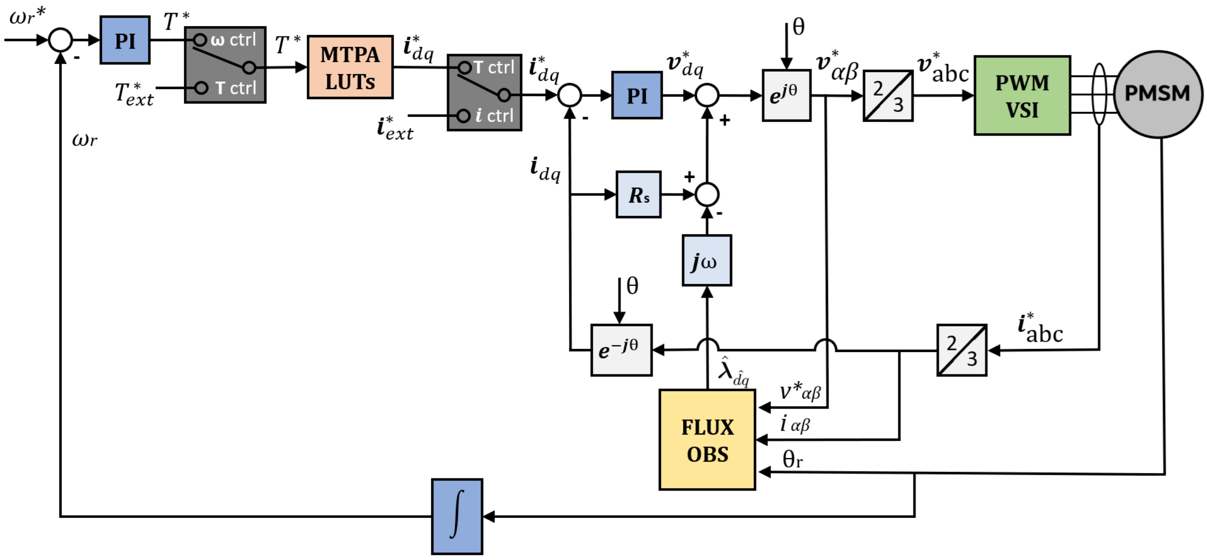

Figure 4.3: Generic FOC scheme for PMSMs

Field-Oriented Control is also characterized by the presence of a flux observer, which plays a crucial role in estimating the magnetic flux necessary for decoupling the control of the motor's torque and magnetizing current. This decoupling allows for independent control of the motor's d-axis and q-axis components, significantly improving performance. Without an accurate flux estimation, the full potential of advanced control strategies cannot be realized, leading to suboptimal efficiency, reduced dynamic response, and limited overall performance of the system.

A flux observer is an advanced algorithm used in electrical drives, to dynamically reconstruct the motor's magnetic flux in real-time. It typically relies on a real-time feedback from voltage and current sensors and a mathematical model of the motor used as feedback loop to compensate for model inaccuracies and disturbances.

Initially to be able to test the model motor model, a simplified version of the flux observer presented in [7] has been used, as shown in Figure∼4.4.

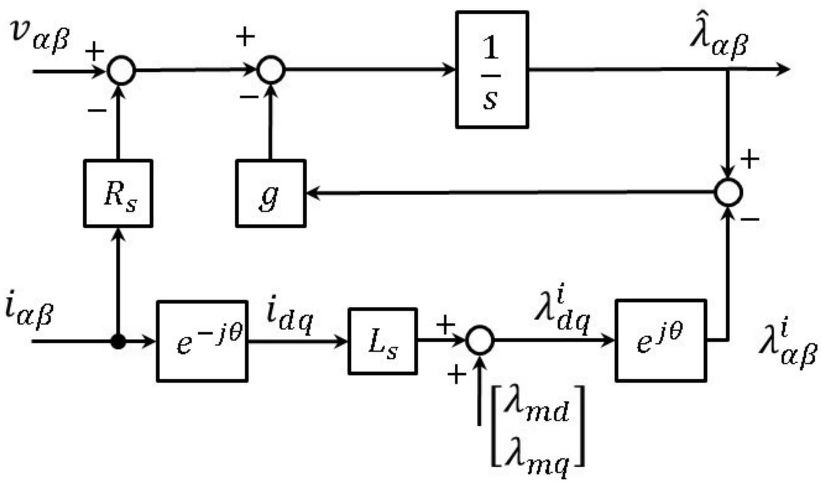

Figure 4.4: Simplified scheme of the flux observer

Considering the 18 to determine the magnet flux, a simulation exploit has been used to acquire the MS and MS_{phase} directly from the motor model, in absence of an observer or estimator to determine them. In the next section will be discussed the implemented method to estimate those quantities.

4.3 MS phase estimate via flux observer

For the real control of a VF-PMSM, with the characteristic analyzed along this work, it is mandatory to implement a precise and robust flux observer. Which also need to be able to estimate the magnetization state (MS) and its phase (MS_{phase}).

The estimation of the magnetization state belongs to the class of problems associated with flux observers, instead the estimation of its phase is more closely related to those concerning position observers, because estimate the MS_{phase} corresponds to estimate the orientation of the magnetic flux vector in space, which is similar to how a position observer estimates the rotor angle.

4.3.1 Active flux

Active flux is a generalized and simplified position error estimation method, presented in 2011 [1]. Active flux refers to the flux component that interacts with the stator current to generate electromagnetic torque, Unlike conventional flux models that account for machine saliency, the active flux approach transforms all salient-pole AC machines into fictitious non-salient-pole machines. This transformation eliminates the complexities associated with magnetic anisotropy, making rotor position and speed estimation more straightforward.
The active flux vector is defined as:

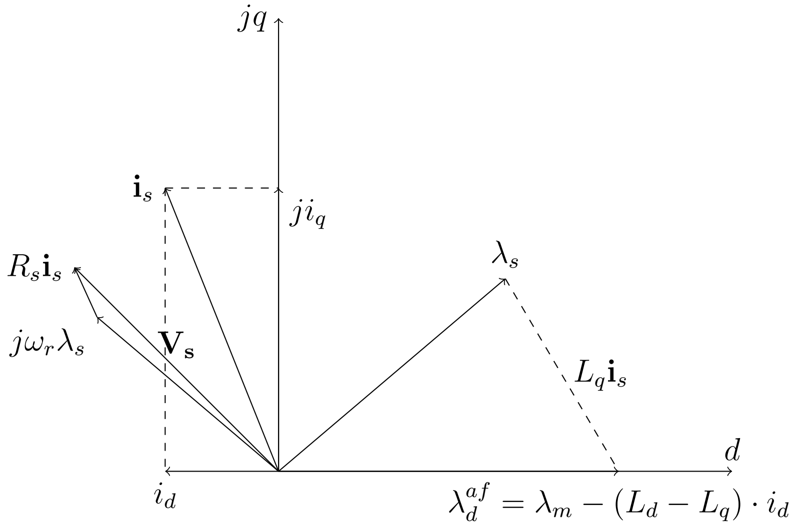

Figure 4.5: Active flux

$$\lambda^{af} = \lambda_s - L_q \cdot \mathbf{i}_s \tag{21}$$

$$\begin{cases} \lambda_d = L_d i_d + \lambda_m \\ \lambda_q = L_q i_q \end{cases} \rightarrow \begin{cases} \lambda_d^{af} = (L_d - L_q) i_d + \lambda_m \\ \lambda_q^{af} = 0 \end{cases} \tag{22}$$

In this particular application, it is essential that, in the case of asymmetrical magnetization, the active flux does not remain aligned with the d-axis, but still remaining equal to the permanent magnets' flux. Because the angle to estimate is the MS_{phase}, which is the magnet flux vector phase angle.

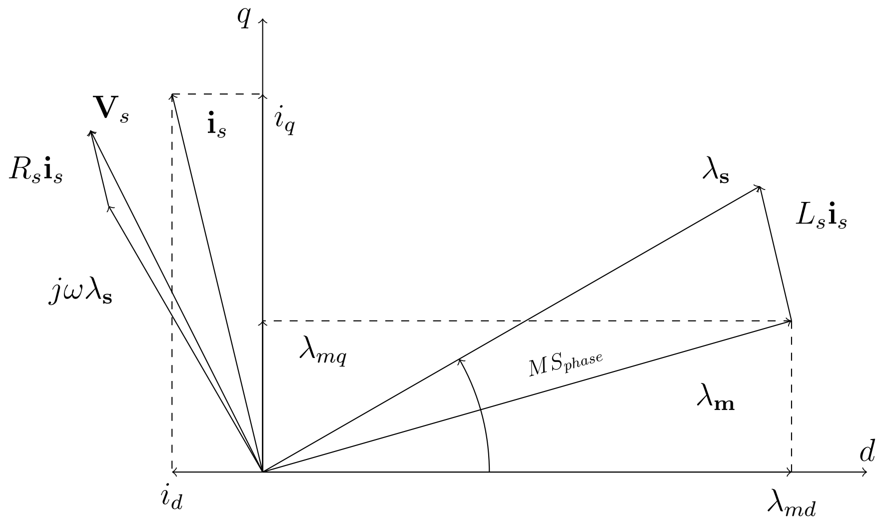

Figure 4.6: VF-PMSM phase vector diagram

By distinguishing the estimated quantities from the measured ones, the formulation is derived as follows.

$$\begin{cases} \hat{\lambda_{dm}} = \hat{\lambda_d} - L_d \cdot i_d \\ \hat{\lambda_{qm}} = \hat{\lambda_q} - L_q \cdot i_q \end{cases} \tag{23}$$

$$\begin{cases} \hat{\lambda_{dm}} = \hat{\lambda_d} - L_d \cdot i_d = \hat{MS}\lambda_{m,MAX} \cdot \cos{(\hat{MS_{phase}})} \\ \hat{\lambda_{qm}} = \hat{\lambda_q} - L_q \cdot i_q = \hat{MS}\lambda_{m,MAX} \cdot \sin{(\hat{MS_{phase}})} \end{cases} \tag{24}$$

$$\begin{cases} \hat{MS} = \dfrac{\sqrt{\hat{\lambda_{dm}}^2 + \hat{\lambda_{qm}}^2}}{\lambda_{m,MAX}} \\ \hat{MS_{phase}} = \arctan{(\dfrac{\hat{\lambda_{qm}}}{\hat{\lambda_{dm}}})} \end{cases} \tag{25}$$

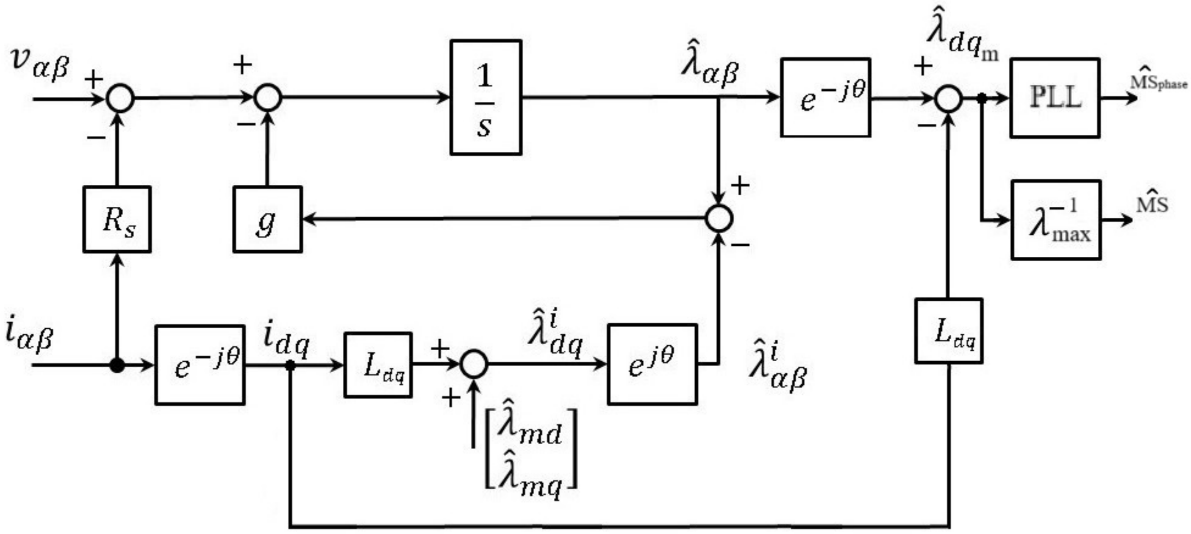

Figure 4.7: Flux observer with MS and MS_{phase} estimator

However, the adopted solution has a significant limitation, as the observer relies on the integration of the back-EMF, which is effective only in the medium-to-high velocity range.

4.3.2 Phase Locked Loop

Most of the sensorless control scheme adopt a PLL because it allows to filtered the estimated position and at the same time retrieve the angular speed. In the Figure~ 4.8 a basic representation of a PLL is shown.

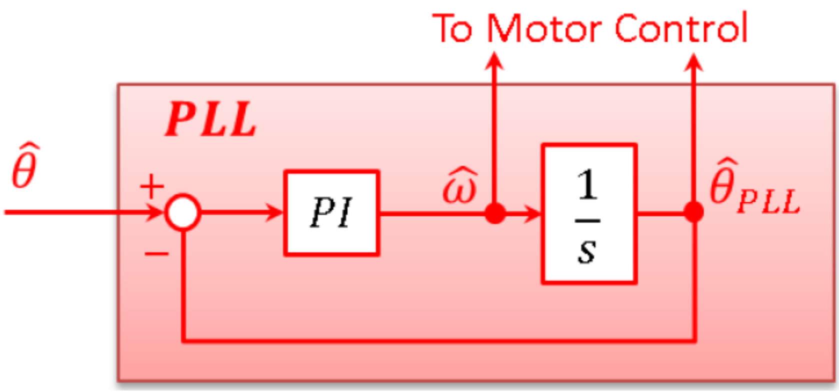

Figure 4.8: PLL scheme

A Phase-Locked Loop is basically a closed loop control system that continuously adjusts its output position and speed to match the input signal. The input $\hat{\theta}$ represents the estimated rotor position , in this case the $\hat{MS}_{phase}$, the value is compared with the PLL's internally generated position $\hat{\theta_{PLL}}$ producing an error signal. The error the error is fed into the PI controller which returns the estimated speed, ensuring that the error is minimized over time. The estimated speed is then integrated to obtain the estimated position which will be sent back to close the feedback loop.

Even though there is no need for estimated speed in this application, it is still preferable to use a PLL rather than a simple low-pass filter. Because the The PLL actively tracks the phase and corrects deviations, making it more responsive to dynamic conditions.

4.3.3 Observer simulation results

The previously described flux observer along with the MS and MS_phase estimator has been tested to evaluate its capability. As done previously for the comparison between the FEA and Simulink models, the machine is also driven to the desired speed in this test , in particular at : 500 rpm, 1000 rpm, 1500 rpm, 2000 rpm and 2500 rpm. The choice to test the observer at different speeds is due to the fact that the observer used is based on the integral of the back-EMF, which is effective primarily at medium to high speeds. Identical current pulses were applied at each speed, once reached the steady state, to assess the observer's ability to accurately estimate MS, MS_{phase} and the fluxes.

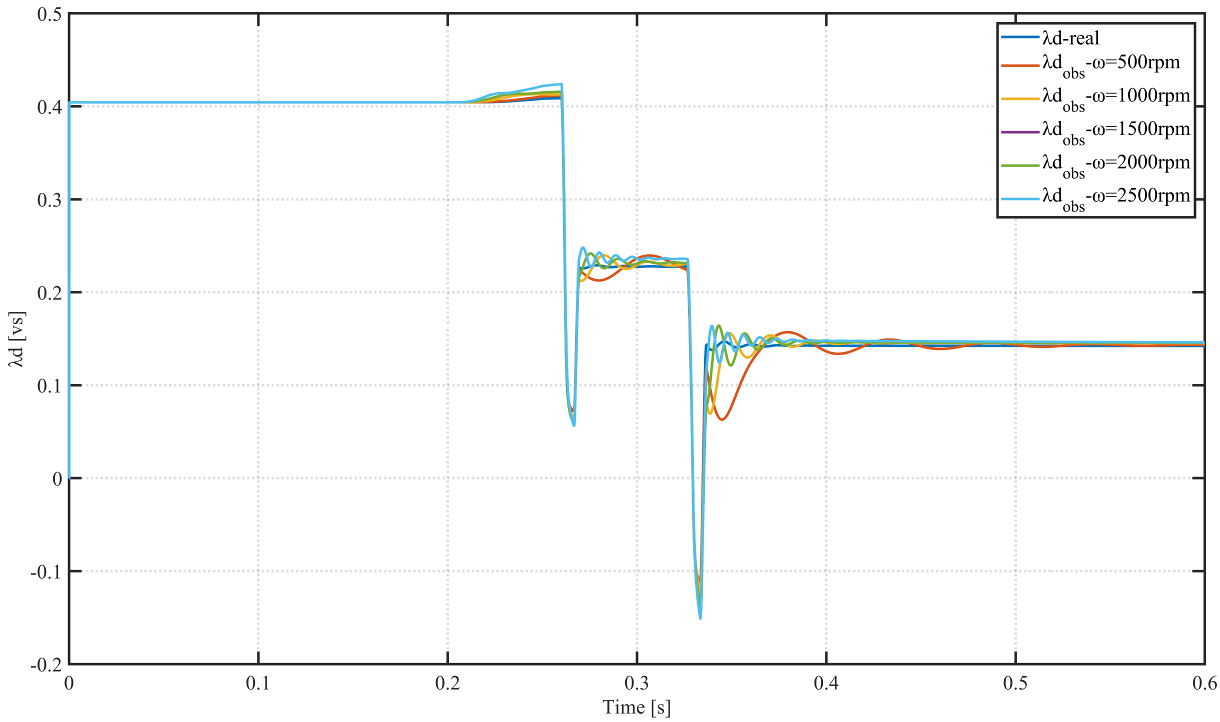

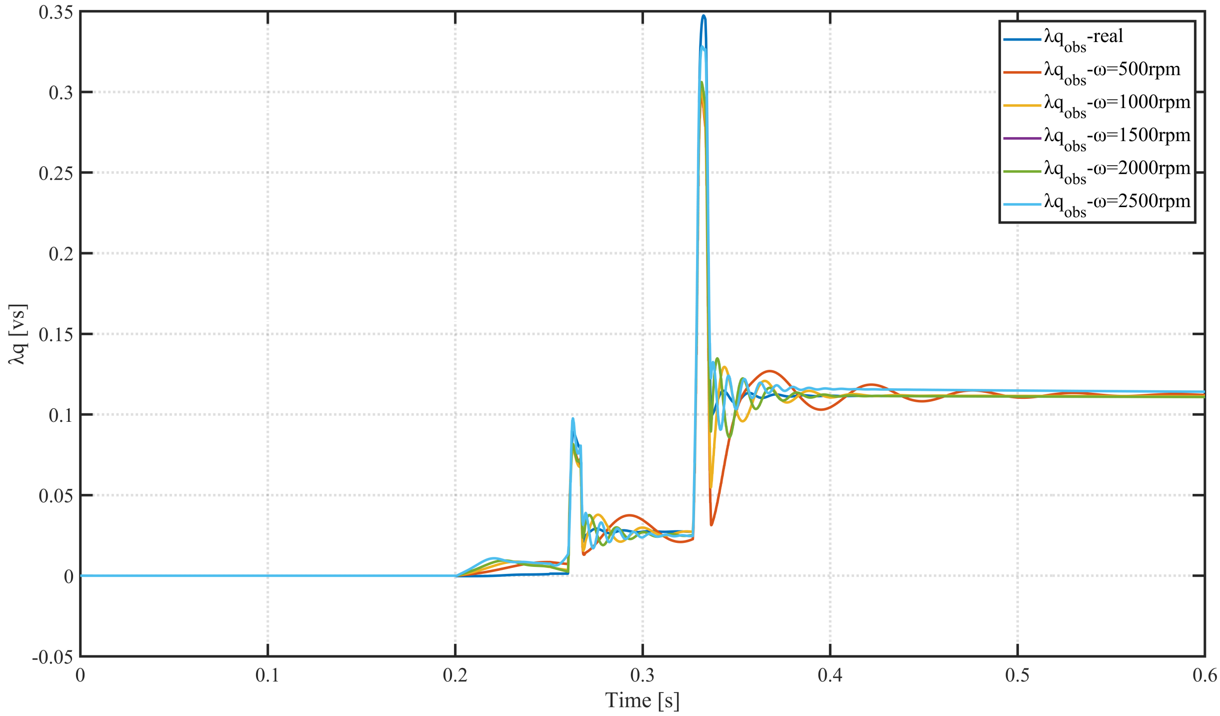

Figure 4.9: Observed Fluxes in dq reference frame

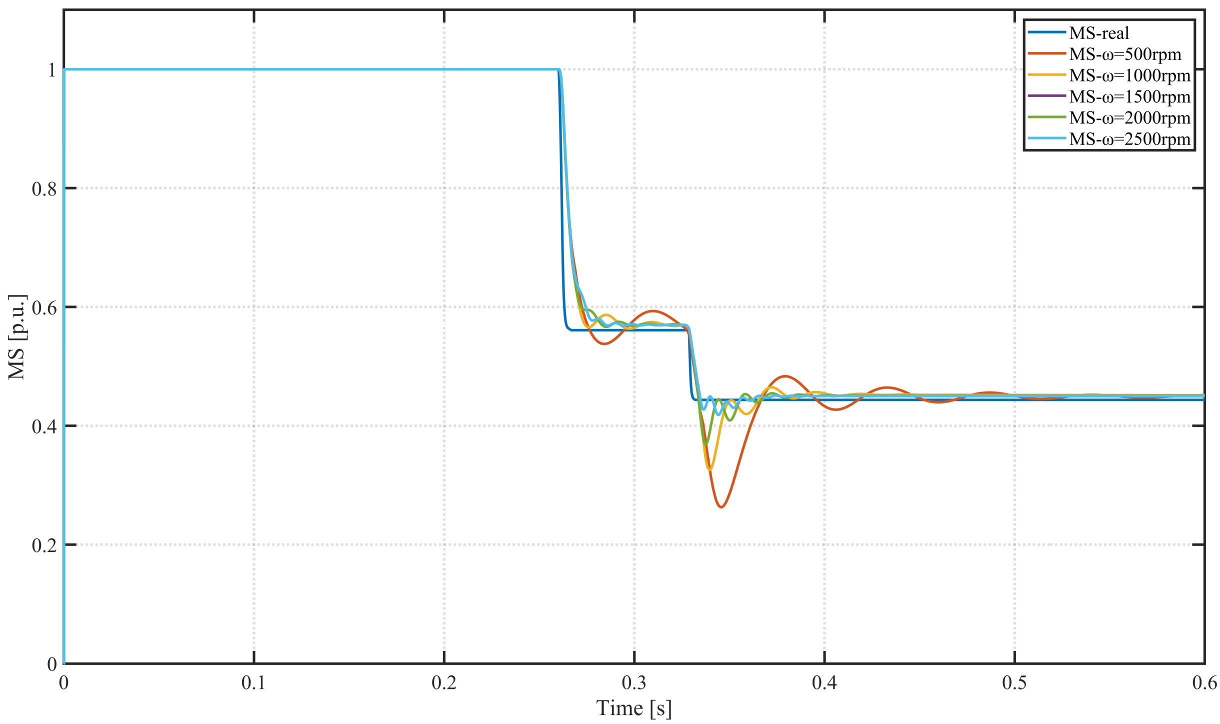

Figure 4.10: Estimated Magnetization State

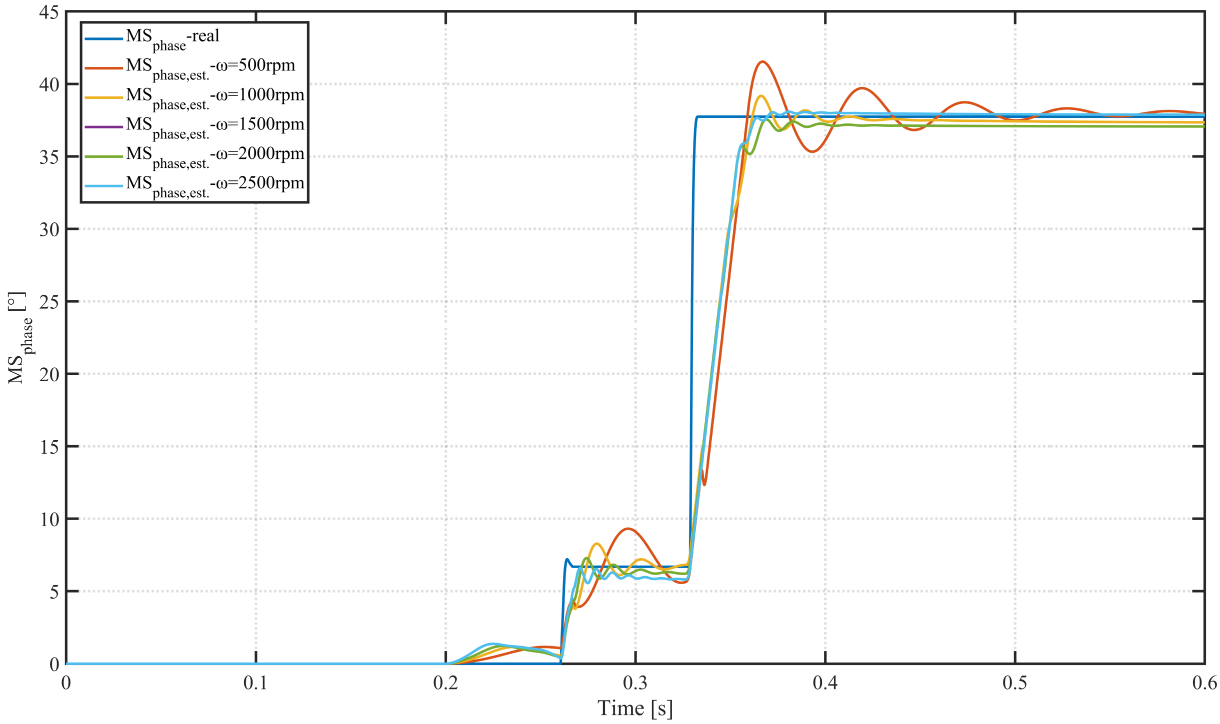

Figure 4.11: Estimated Magnetization State Phase

As previously mentioned, the observer performs better in the medium to high-speed range, showing a significant improvement in results between 500 rpm and 2500 rpm. Regarding the phase estimator, its dynamic response is highly dependent on the parameters of the PLL's PI controller. In this case, they were deliberately set to slightly overdamp the response, as this configuration proved to work better during the actual control of the machine. Furthermore, for comparison purposes, the parameters of both the PI controller and the feedback gain g were kept constant across all speeds. However, to improve the response, a good solution would be to use values that adapt as a function of speed. In conclusion, despite the evident improvements needed to achieve more stable control, the observer is capable of estimating the fluxes, MS and MS_{phase} with a steady-state error of less than 5%, allowing it to be effectively used in the control of the machine, as will be shown in the next section.

4.4 Modified FOC in dq-m reference frame

The newly proposed variation of the Field Oriented Control, is based on the previously presented observer. Specifically designed for VF-PMSMs, in a condition of symmetrical magnetization has the same orientation of the dq reference frame using the rotor position for the transform. Than in case of uneven magnetization, and by so a misalignment of the $\lambda_{\mathbf{m}}$ respect the d-axis, the new FOC use the estimated value $\hat{MS_{phase}}$ to compensate this angle and realign the d-axis, renamed for this case d_m-axis, realigning to the magnet flux vector.

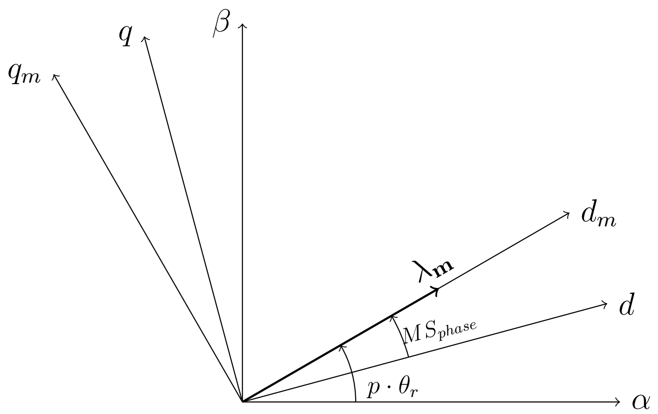

Figure 4.12: dq_m Reference frame definition

As can be seen from Figures~ 4.13,4.14, obtained driving the machine into rotation and subsequently applying two demagnetization pulses, the first only along the d-axis to achieve homogeneous demagnetization, and the second to obtain asymmetric magnetization. The flux appears identical in both reference frames as long as the magnetization remains homogeneous. However, when the phase component MS_{phase} becomes different from zero, a flux component appears in the q-axis, beyond the one observed during the pulses. Instead, thanks to the compensation of the new reference frame, this component remains zero in the dq_m reference frame.

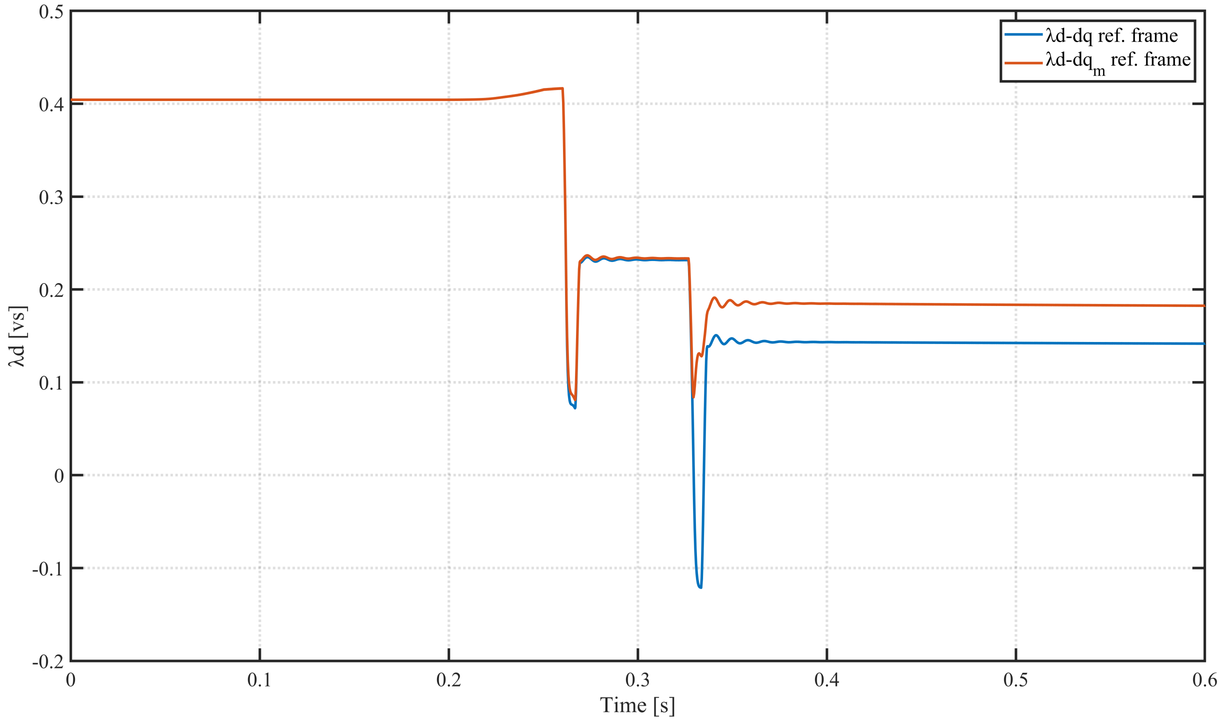

Figure 4.13: λ_d in dq and dq_m ref. frame

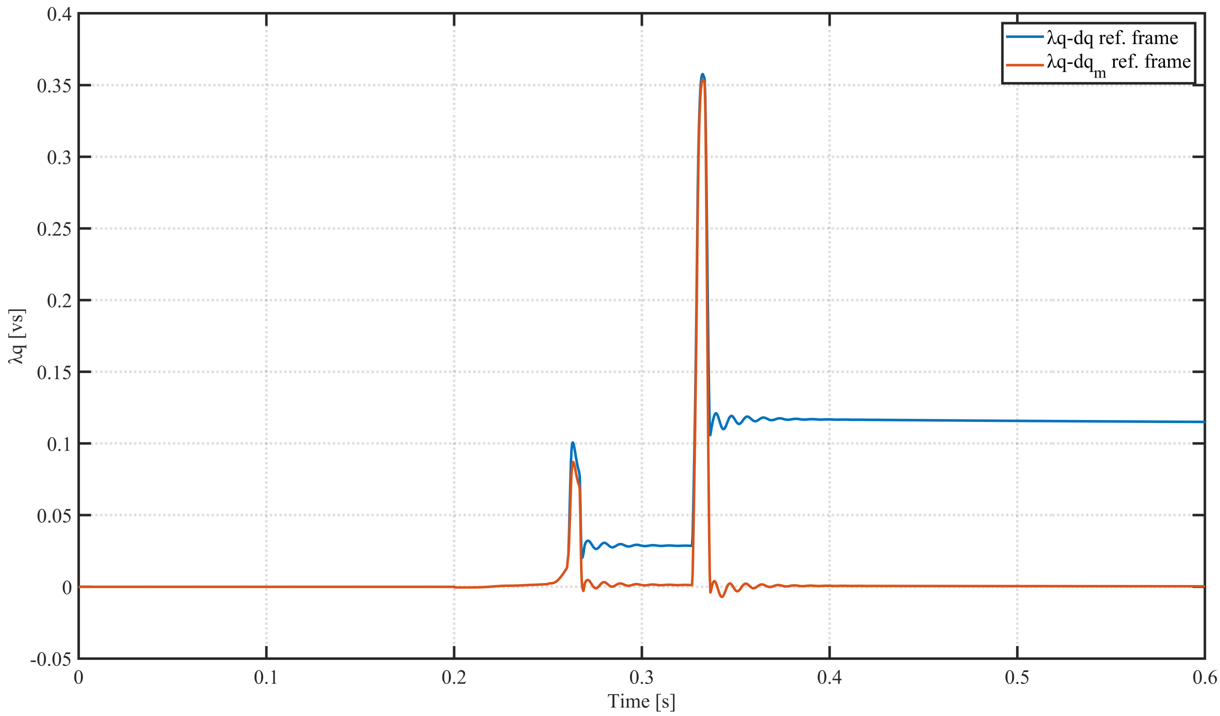

Figure 4.14: λ_q in dq and dq_m ref. frame

Considering the control of the machine following, a simplified, Maximum Torque Per Ampere strategy of an SPM motor, that means setting the d-axis current to zero to maximize the availability of current on the q-axis for torque generation, based on 13, this means imposing a current in quadrature with the magnet flux to maximize the generated torque. In the case of asymmetric magnetization, when using traditional Field-Oriented Control, the q-axis is no longer in quadrature with the magnet flux. This misalignment results in a deviation from the MTPA, leading to less precise and less efficient torque control.

To demonstrate this, a test was conducted starting from the same magnetization conditions, with $MS = 60\%$ and $MS_{phase} = 20°$, the machine is driven to a speed of 1500 rpm through speed control, followed by a load application of 10 Nm, first in the dq reference frame and then in the dq_m. To effectively compare the performance of the two control strategies, the speed dynamics, th torque accuracy and the stator Joule losses were evaluated, which also corresponds to analyzing the magnitude of the current required to achieve the torque.

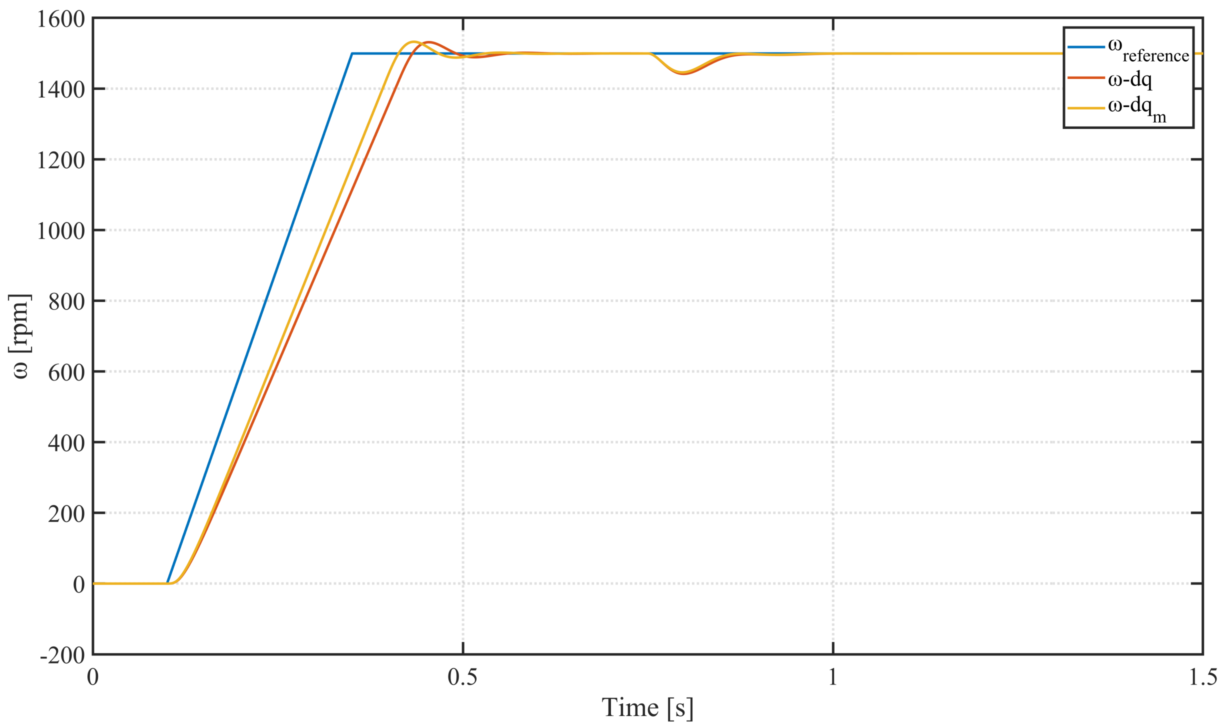

Figure 4.15: Speed comparison

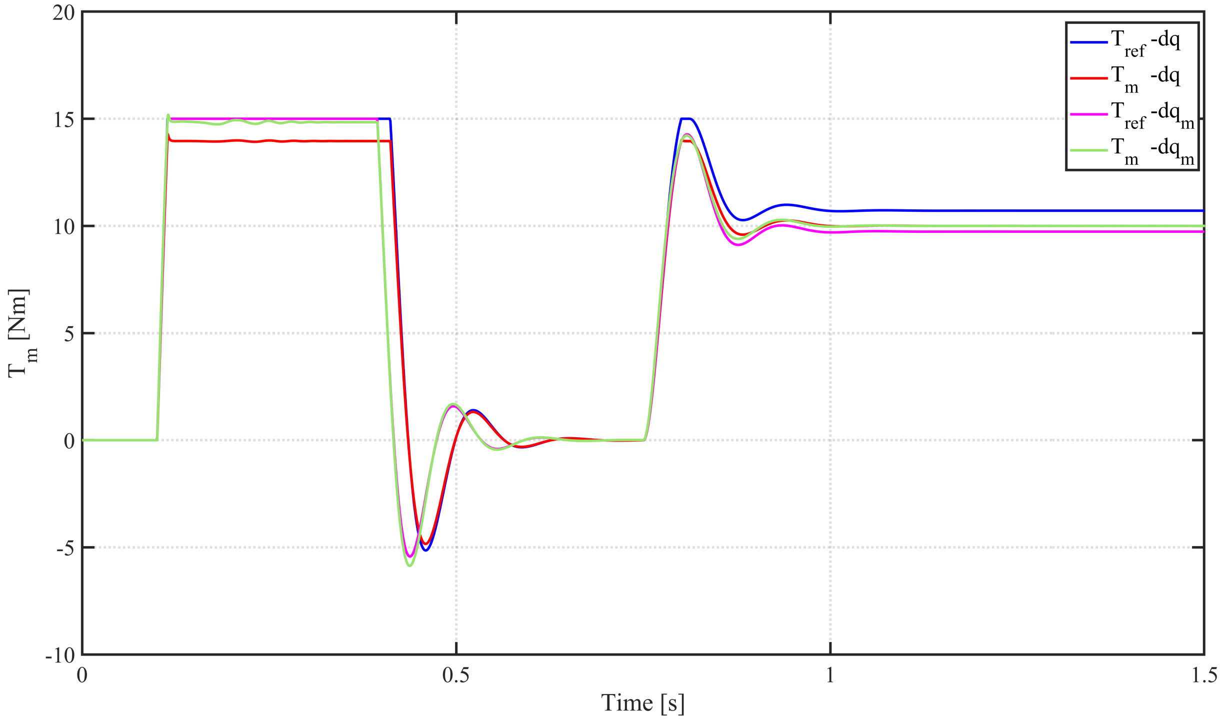

Figure 4.16: Torque comparison

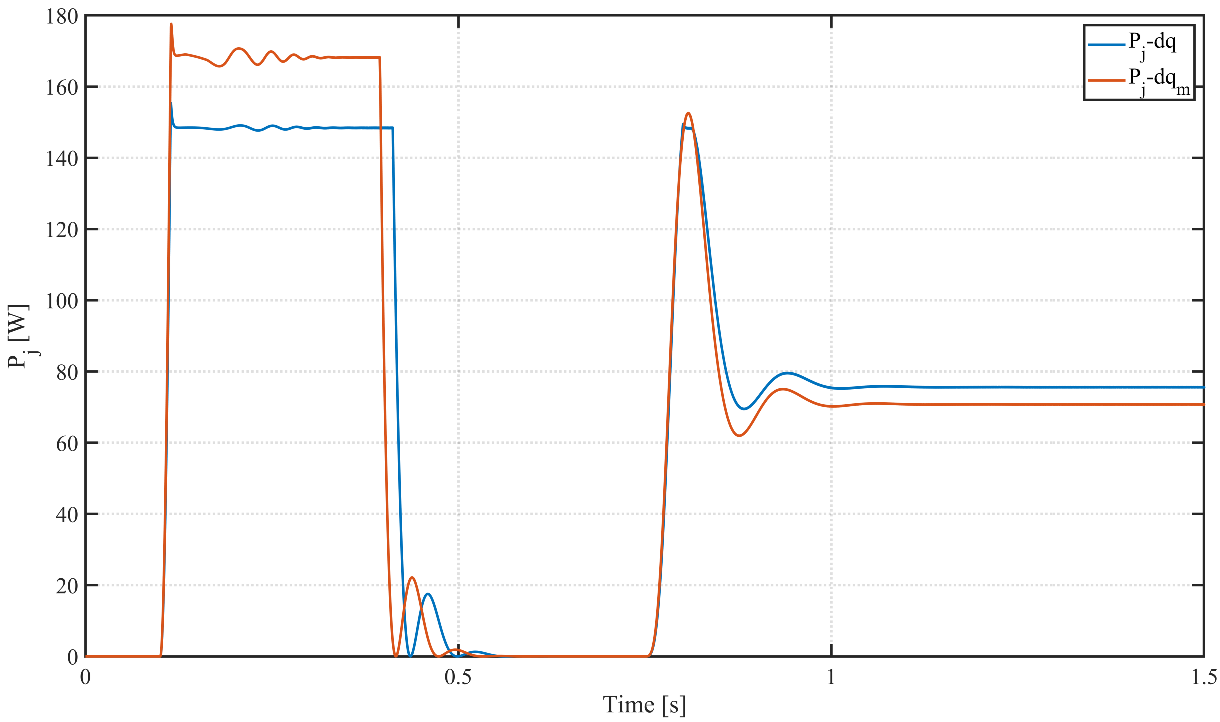

Figure 4.17: Joule losses comparison

The simulation was conducted while maintaining the same control parameters for both dq and dq_m Field Oriented Control. As shown in Figure ~ 4.15, the control in the dq_m reference frame exhibits slightly faster dynamics.

This increased dynamic response is due to the higher torque achieved during the acceleration phase, as illustrated in Figure $\sim$ 4.16. Although the torque reference set by the PI controller remains the same for both cases, the dq reference frame fails to reach it, because the d-axis isn't properly aligned whit $\lambda_{\mathbf{m}}$, while the dq_m control ensure a proper alignment, having the q_m-axis current in quadrature withe the magnet flux, following the MTPA, as suggested by13. Consequently, the reference torque in the dq_m case decreases earlier, reaching the required speed. While in the second phase, the load pickup, , both methods successfully achieve the required 10 Nm. However, in the dq reference frame, the PI controller demands a significantly higher reference torque, requiring more current to compensate.

From the losses perspective, the higher torque leads into increased losses, as shown in Figure $\sim$ 4.17, but for a shorter period of time. While in the load pickup, the dq_m control achieves a noticeable reduction in losses. While the total energy losses in the simulation are nearly identical, with the dq_m control providing only a 0.309% improvement, if we consider only the load pickup the modified FOC approach results in a 6.05% reduction in losses.This means that, for the same dynamic performance, the FOC in the dq_m reference frame ensures a significant improvement in efficiency.

5 Conclusion and future development

The primary objective of this thesis was to develop a novel model for Variable Flux Permanent Magnet Synchronous Machines (VF-PMSMs) that accounts for asymmetrical magnetization. This model was then utilized to design an observer and a control scheme for efficient operation under such conditions.

The thesis follows two main lines of investigation:

- **1) Development of fast and accurate simulation model covering asymmetrical demagnetization**

  The intrinsic demagnetization capability of VF-PMSMs poses several challenges to its modeling, simulation and control. For this reason, the available simulation models normally exploits co-simulation techniques, where the machine is represented through Finite Elements Analysis (FEA). This leads to very high computational burden and simulation time, incompatible with the motor control development and calibration. A Simulink model was developed in [5]capable of describing the demagnetization phenomena but limited to uniform magnetization of the PMs.

  To solve this issue, the thesis begins with an introduction to VF-PMSMs, accompanied by a mathematical dynamic model, which serves as a foundational framework for understanding their behavior. Following this, an extensive explanation of the Simulink model in [5] is provided, as it serves as a base for developing the new model. This is followed by an analysis of the asymmetrical magnetization behavior and the methodologies employed for modeling this phenomenon.

  Two versions of the model were developed. The first is a simplified and linearized model based on constant inductances, tailored to the characteristics of the machine under test. The second is a refined version based on armature flux maps, thus covering magnetic saturation and cross-saturation. Both the models are capable of describing the machine behavior even in the case of asymmetrical demagnetization. The developed models were extensively tested and compared with both the initial model and a finite element model to verify their correctness and accuracy across all operational areas.

- **2) Control development**

  The asymmetrical demagnetization poses potential issues on motor torque control stability and accuracy. Given the unique characteristics of these machines, a flux observer was developed to estimate not only the machine's flux but also the magnitude and phase of the magnetization state. This information is crucial for determining the symmetry or asymmetry of magnetization in the magnets. The observer, capable of operating only in the medium and high speed range, is based on the compensation of the armature flux linkage.

  Based on this observer, a Modified Field Oriented Control strategy was proposed, which accounts for possible magnetization asymmetry to maximize efficiency. This strategy adapts the current vector direction to the eventual asymmetry in the magnetization, guaranteeing torque accuracy and minimum Joule losses even in this scenario.

Future activities

As VF-PMSMs are a relatively new and continuously evolving class of electrical machines, there are multiple avenues for future development. Key aspects that were not covered in this thesis but could provide immediate expansion opportunities include:

- Validation of the Developed Model: Validating the model with a real prototype of the machine under test (MUT) to obtain actual magnetization and demagnetization maps.
- Observer Development: Creating an observer capable of accurately estimating modulation state (MS) and MS phase values at low speeds and during standstill.
- Magnetization State Control Strategy: Implementing a control strategy to manage the magnetization state, maximizing machine efficiency based on operating conditions.

The content of this thesis has been included in a conference paper recently submitted for possible publication at the next IEEE Energy Conversion Congress and Exposition (ECCE 2025), planned to be host in Philadelphia in October 2025.

References

[1] I. Boldea and S. C. Agarlita. The active flux concept for motion-sensorless unified ac drives: A review. In *International Aegean Conference on Electrical Machines and Power Electronics and Electromotion, Joint Conference*, pages 1–16, 2011.

[2] Huang Jia, Wang Xinjian, and Sun Zechang. Variable flux memory motors: A review. In *2014 IEEE Conference and Expo Transportation Electrification Asia-Pacific (ITEC Asia-Pacific)*, pages 1–6, 2014.

[3] Natee Limsuwan, Takashi Kato, Kan Akatsu, and Robert D. Lorenz. Design and evaluation of a variable-flux flux-intensifying interior permanent-magnet machine. *IEEE Transactions on Industry Applications*, 50(2):1015–1024, 2014.

[4] Wei Liu, Hui Yang, Heyun Lin, and Xiping Liu. Influence of low-coercive-force magnet property on electromagnetic performance of variable flux memory machine. *IEEE Transactions on Magnetics*, 58(8):1–6, 2022.

[5] Maedeh Sadat Mirazimi, Chen Chen, Paolo Pescetto, Simone Ferrari, Gianmario Pellegrino, Michela Diana, and Torbjörn Thiringer. Accurate modeling of variable- flux pmsms without electromagnetic co-simulation. In *2024 International Symposium on Power Electronics, Electrical Drives, Automation and Motion (SPEEDAM)*, pages 625–630, 2024.

[6] V. Ostovic. Memory motors-a new class of controllable flux pm machines for a true wide speed operation. In *Conference Record of the 2001 IEEE Industry Applications Conference. 36th IAS Annual Meeting (Cat. No.01CH37248)*, volume 4, pages 2577–2584 vol.4, 2001.

[7] Gianmario Pellegrino, Radu Iustin Bojoi, and Paolo Guglielmi. Unified direct-flux vector control for ac motor drives. *IEEE Transactions on Industry Applications*, 47(5):2093–2102, 2011.

[8] G. Pellegrino S. Ferrari, F. Cupertino. SyR-e Software, 2014. https://github.com/SyR-e.

[9] Anantaram Varatharajan, Dario Brunelli, Simone Ferrari, Paolo Pescetto, and Gianmario Pellegrino. syredrive: Automated sensorless control code generation for synchronous reluctance motor drives. In *2021 IEEE Workshop on Electrical Machines Design, Control and Diagnosis (WEMDCD)*, pages 192–197, 2021.